

THESIS FOR THE DEGREE OF DOCTOR OF PHILOSOPHY

---

Compensation of Laser Phase Noise Using DSP in  
Multichannel Fiber-Optic Communications

ARNI F. ALFREDSSON



**CHALMERS**  
UNIVERSITY OF TECHNOLOGY

Communication Systems Group  
Department of Electrical Engineering  
Chalmers University of Technology  
Göteborg, Sweden, 2020

**Compensation of Laser Phase Noise Using DSP in  
Multichannel Fiber-Optic Communications**

ARNI F. ALFREDSSON

ISBN 978-91-7905-267-6

Copyright © 2020 ARNI F. ALFREDSSON, except where  
otherwise stated. All rights reserved.

Doktorsavhandlingar vid Chalmers tekniska högskola  
Ny serie nr 4734  
ISSN 0346-718X

This thesis has been prepared using L<sup>A</sup>T<sub>E</sub>X and Tikz.

Communication Systems Group  
Department of Electrical Engineering  
Chalmers University of Technology  
SE-412 96 Göteborg, Sweden  
Phone: +46 (0)31 772 1000  
[www.chalmers.se](http://www.chalmers.se)

Front cover illustration:  
Correlated phase noise in 3 cores of a multicore fiber.  
Based on the experimental data used in Paper C.

Printed by Chalmers Reproservice  
Göteborg, Sweden, March 2020

# Abstract

One of the main impairments that limit the throughput of fiber-optic communication systems is laser phase noise, where the phase of the laser output drifts with time. This impairment can be highly correlated across channels that share lasers in multichannel fiber-optic systems based on, e.g., wavelength-division multiplexing using frequency combs or space-division multiplexing. In this thesis, potential improvements in the system tolerance to laser phase noise that are obtained through the use of joint-channel digital signal processing are investigated. To accomplish this, a simple multichannel phase-noise model is proposed, in which the phase noise is arbitrarily correlated across the channels. Using this model, high-performance pilot-aided phase-noise compensation and data-detection algorithms are designed for multichannel fiber-optic systems using Bayesian-inference frameworks. Through Monte Carlo simulations of coded transmission in the presence of moderate laser phase noise, it is shown that joint-channel processing can yield close to a 1 dB improvement in power efficiency. It is further shown that the algorithms are highly dependent on the positions of pilots across time and channels. Hence, the problem of identifying effective pilot distributions is studied.

The proposed phase-noise model and algorithms are validated using experimental data based on uncoded space-division multiplexed transmission through a weakly-coupled, homogeneous, single-mode, 3-core fiber. It is found that the performance improvements predicted by simulations based on the model are reasonably close to the experimental results. Moreover, joint-channel processing is found to increase the maximum tolerable transmission distance by up to 10% for practical pilot rates.

Various phenomena decorrelate the laser phase noise between channels in multichannel transmission, reducing the potency of schemes that exploit this correlation. One such phenomenon is intercore skew, where the spatial channels experience different propagation velocities. The effect of intercore skew on the performance of joint-core phase-noise compensation is studied. Assuming that the channels are aligned in the receiver, joint-core processing is found to be beneficial in the presence of skew if the linewidth of the local oscillator is lower than the light-source laser linewidth.

In the case that the laser phase noise is completely uncorrelated across channels in multichannel transmission, it is shown that the system performance can be improved by applying transmitter-side multidimensional signal rotations. This is found by numerically optimizing rotations of four-dimensional signals that are transmitted through two channels. Structured four-dimensional rotations based on Hadamard matrices are found to be near-optimal. Moreover, in the case of high signal-to-noise ratios and high signal dimensionalities, Hadamard-based rotations are found to increase the achievable information rate by up to 0.25 bits per complex symbol for transmission of higher-order modulations.

**Keywords:** Coherent fiber-optic communications, digital signal processing, detection, estimation, multichannel transmission, laser phase noise, rotations.



## List of Publications

This thesis is based on the following publications:

- [A] **A. F. Alfredsson**, E. Agrell, and H. Wymeersch, “Iterative detection and phase-noise compensation for coded multichannel optical transmission,” *IEEE Transactions on Communications*, vol. 67, no. 8, pp. 5532–5543, Aug. 2019.
- [B] **A. F. Alfredsson**, E. Agrell, M. Karlsson, and H. Wymeersch, “Pilot distributions for joint-channel carrier-phase estimation in multichannel optical communications,” submitted to *IEEE/OSA Journal of Lightwave Technology*, Feb. 2020.
- [C] **A. F. Alfredsson**, E. Agrell, H. Wymeersch, B. J. Puttnam, G. Rademacher, R. S. Luís, and M. Karlsson, “Pilot-aided joint-channel carrier-phase estimation in space-division multiplexed multicore fiber transmission,” *IEEE/OSA Journal of Lightwave Technology*, vol. 37, no. 4, pp. 1133–1142, Feb. 2019.
- [D] **A. F. Alfredsson**, E. Agrell, M. Karlsson, and H. Wymeersch, “On the performance of joint-core carrier-phase estimation in the presence of intercore skew,” *IEEE/OSA Journal of Lightwave Technology*, vol. 37, no. 20, pp. 5291–5298, Oct. 2019.
- [E] **A. F. Alfredsson**, E. Agrell, M. Karlsson, and H. Wymeersch, “Optimization of transmitter-side signal rotations in the presence of laser phase noise,” submitted to *IEEE/OSA Journal of Lightwave Technology*, Dec. 2019.

Publications by the author not included in the thesis:

- **A. F. Alfredsson**, R. Krishnan, and E. Agrell, “Joint-polarization phase-noise estimation and symbol detection for optical coherent receivers,” *IEEE/OSA Journal of Lightwave Technology*, vol. 34, no. 18, pp. 4394–4405, Sep. 2016.
- **A. F. Alfredsson**, E. Agrell, H. Wymeersch, and M. Karlsson, “Phase-noise compensation for spatial-division multiplexed transmission,” in *Proc. Optical Fiber Communication Conference (OFC)*, Mar. 2017, paper Th4C.7.
- **A. F. Alfredsson**, E. Agrell, H. Wymeersch, and M. Karlsson, “Pilot distributions for phase tracking in space-division multiplexed systems,” in *Proc. European Conference on Optical Communication (ECOC)*, Sep. 2017, paper P1.SC3.48.
- E. Agrell, **A. F. Alfredsson**, B. J. Puttnam, and R. S. Luís, G. Rademacher, and M. Karlsson, “Modulation and detection for multicore superchannels with correlated phase noise,” (invited paper) in *Proc. Conference on Lasers and Electro-Optics (CLEO)*, May 2018, paper SM4C.3.
- **A. F. Alfredsson**, E. Agrell, H. Wymeersch, B. J. Puttnam, G. Rademacher, and R. S. Luís, “Joint phase tracking for multicore transmission with correlated phase noise,” (invited paper) in *Proc. IEEE Summer Topicals Meeting Series (SUM)*, Jul. 2018, paper MF1.2.
- **A. F. Alfredsson**, “Phase-noise compensation for space-division multiplexed multicore fiber transmission,” Gothenburg, Sweden, Licentiate Thesis, Sep. 2018.
- B. J. Puttnam, R. S. Luís, G. Rademacher, **A. F. Alfredsson**, W. Klaus, J. Sakaguchi, Y. Awaji, E. Agrell, and N. Wada, “Characteristics of homogeneous multicore fibers for SDM transmission,” (invited paper) *APL Photonics*, vol. 4, no. 2, p. 022804, Feb. 2019.
- **A. F. Alfredsson**, E. Agrell, H. Wymeersch, and M. Karlsson, “On the impact of intercore skew on joint-core carrier-phase estimation,” in *Proc. European Conference on Optical Communication (ECOC)*, Sep. 2019, paper Tu.3.B.4.

## Acknowledgments

First and foremost, I would like to express my gratitude to Prof. Erik Agrell for seeing the potential in me and offering me a PhD position at Chalmers. I might not even have decided to pursue a PhD if it had not been for you. Five excellent years have passed since we started working together and you have taught me a great deal about what it means to do research. Moreover, Prof. Henk Wymeersch has been instrumental in my progress and has been especially helpful with all things Bayesian, which I highly appreciate. I would also like to thank Prof. Magnus Karlsson for the discussions we have had over the years, which have given me a lot of insight into fiber-optic communications. Finally, I want to thank Dr. Pontus Johannisson for his help in the beginning of my PhD studies.

Big thanks go to my collaborators at the National Institute of Information and Communications Technology who provided me with experimental data that greatly benefited my work. I want to specifically acknowledge Dr. Benjamin Puttnam for his all efforts pertaining to the collaboration, as well as Dr. Ruben Luís for assisting me with the signal processing of the experimental data.

Thanks to Prof. Erik Ström and Prof. Fredrik Brännström for their ambitions in improving the working environment at Chalmers, as well as to the administration staff for their help. Moreover, I want to acknowledge all my colleagues in the FORCE group for providing a diverse and challenging working environment. Special thanks go to the people in the CS group for making the workplace awesome.

I am grateful to my family who has always been very supportive and interested in my life. Last but not least, huge thanks go to Jóhanna for her motivation and patience during my time at Chalmers. Takk fyrir allt ást! I am excited to see what the future has in store for us.

Arni F. Alfreðsson  
Göteborg, 2020

## **Financial Support**

This work was supported by the Swedish Research Council (VR) under grants 2013-5642, 2014-6138, and 2018-03701, as well as by the Knut and Alice Wallenberg Foundation under Grant 2018.0090. Moreover, I would like to acknowledge Ericsson's Research Foundation for partially funding my research travels.

# Acronyms

<b>AIR</b>	achievable information rate
<b>ASE</b>	amplified spontaneous emission
<b>AWGN</b>	additive white Gaussian noise
<b>BER</b>	bit error rate
<b>BLER</b>	block error rate
<b>BPS</b>	blind phase search
<b>CD</b>	chromatic dispersion
<b>CMA</b>	constant modulus algorithm
<b>DSP</b>	digital signal processing
<b>FEC</b>	forward error correction
<b>FG</b>	factor graph
<b>FIR</b>	finite impulse response
<b>FWM</b>	four-wave mixing
<b>GMI</b>	generalized mutual information
<b>LDPC</b>	low-density parity-check
<b>LLR</b>	log-likelihood ratio
<b>LO</b>	local oscillator
<b>LPN</b>	laser phase noise
<b>MAP</b>	maximum <i>a posteriori</i>
<b>MCF</b>	multicore fiber
<b>MDL</b>	more-dependent loss
<b>MI</b>	mutual information
<b>MIMO</b>	multiple-input multiple-output
<b>MMF</b>	multimode fiber
<b>MSE</b>	mean squared error
<b>PDF</b>	probability density function
<b>PDL</b>	polarization-dependent loss
<b>PDM</b>	polarization-division multiplexing
<b>PMD</b>	polarization-mode dispersion
<b>PMF</b>	probability mass function
<b>PNC</b>	phase-noise compensation
<b>PSK</b>	phase-shift keying
<b>QAM</b>	quadrature amplitude modulation

<b>QPSK</b>	quadrature phase-shift keying
<b>SDM</b>	space-division multiplexing
<b>SER</b>	symbol error rate
<b>SMF</b>	single-mode fiber
<b>SNR</b>	signal-to-noise ratio
<b>SPA</b>	sum-product algorithm
<b>SPM</b>	self-phase modulation
<b>VB</b>	variational Bayesian
<b>WDM</b>	wavelength-division multiplexing
<b>XPM</b>	cross-phase modulation

---

# Contents

---

<b>Abstract</b>	<b>i</b>
<b>List of Papers</b>	<b>iii</b>
<b>Acknowledgments</b>	<b>v</b>
<b>Acronyms</b>	<b>vii</b>
<b>I Overview</b>	<b>1</b>
<b>1 Background</b>	<b>3</b>
1.1 Thesis Organization . . . . .	6
1.2 Notation . . . . .	7
<b>2 Fiber-Optic Communications</b>	<b>9</b>
2.1 Basic System Overview . . . . .	10
2.1.1 The Transmitter . . . . .	11
2.1.2 The Fiber-Optic Channel . . . . .	11
2.1.3 The Coherent Receiver . . . . .	12
2.2 Wavelength-Division Multiplexing . . . . .	13
2.3 Space-Division Multiplexing . . . . .	14
2.3.1 Bundles of Single-Mode Fibers . . . . .	14
2.3.2 Multicore Fibers . . . . .	15
2.3.3 Multimode Fibers . . . . .	16
2.3.4 Multicore–Multimode Fibers . . . . .	17
2.4 Modulation Formats . . . . .	17

2.5	Forward Error Correction . . . . .	19
2.6	Transmission Impairments . . . . .	20
2.6.1	Additive Noise . . . . .	20
2.6.2	Polarization Effects . . . . .	20
2.6.3	Chromatic Dispersion . . . . .	21
2.6.4	Nonlinearities . . . . .	21
2.6.5	Carrier-Frequency Offset and Laser Phase Noise . . . . .	22
2.6.6	I/Q Imbalance . . . . .	24
2.6.7	Propagation Delays between Channels . . . . .	24
2.7	Performance Metrics . . . . .	24
<b>3</b>	<b>Digital Signal Processing</b>	<b>27</b>
3.1	Transmitter DSP . . . . .	27
3.2	Receiver DSP . . . . .	28
3.2.1	Orthonormalization . . . . .	28
3.2.2	Dispersion Compensation . . . . .	29
3.2.3	Adaptive Equalization . . . . .	29
3.2.4	Frequency-Offset Compensation . . . . .	30
3.2.5	Data Detection . . . . .	31
<b>4</b>	<b>Phase-Noise Compensation</b>	<b>33</b>
4.1	Multichannel Phase-Noise Model . . . . .	34
4.2	Optimal Detection in the Presence of Phase Noise . . . . .	34
4.3	Single-Channel Processing . . . . .	36
4.3.1	Blind Algorithms . . . . .	36
4.3.2	Pilot-Aided Algorithms . . . . .	37
4.4	Joint-Channel Processing . . . . .	38
4.4.1	Perfect Phase-Noise Correlation . . . . .	39
4.4.2	Partial Phase-Noise Correlation . . . . .	40
4.4.3	Pilot-Symbol Positions . . . . .	40
<b>5</b>	<b>Contributions</b>	<b>43</b>
5.1	Paper A . . . . .	43
5.2	Paper B . . . . .	44
5.3	Paper C . . . . .	44
5.4	Paper D . . . . .	45
5.5	Paper E . . . . .	45
5.6	Future Work . . . . .	46
	<b>Bibliography</b>	<b>49</b>

## II Papers

71

### A Iterative Detection and Phase-Noise Compensation for Coded Multichannel Optical Transmission **A1**

1	Introduction . . . . .	A3
2	System Model . . . . .	A5
3	Derivation of Algorithms . . . . .	A7
3.1	Phase-Noise Estimation . . . . .	A8
3.2	FG/SPA-Based Algorithm . . . . .	A10
3.3	VB-Based Algorithm . . . . .	A13
3.4	Distribution of Pilot Symbols . . . . .	A17
3.5	Conversion Between PMFs and LLRs . . . . .	A17
3.6	Computational Complexity . . . . .	A18
4	Performance Results . . . . .	A18
4.1	Impact of EKF Linearization . . . . .	A18
4.2	Experimental Verification . . . . .	A19
4.3	Simulation Results . . . . .	A20
5	Discussion and Conclusions . . . . .	A22
A	Derivation of EKF Equations . . . . .	A23
B	Derivation of FG messages . . . . .	A24
	Acknowledgment . . . . .	A25
	References . . . . .	A26

### B Pilot Distributions for Joint-Channel Carrier-Phase Estimation in Multichannel Optical Communications **B1**

1	Introduction . . . . .	B3
2	System Model . . . . .	B5
3	Pilot Distributions . . . . .	B7
3.1	Unstructured Optimization . . . . .	B8
3.2	Structured Optimization . . . . .	B8
3.3	Heuristic Pilot Distributions . . . . .	B8
4	Numerical Results . . . . .	B9
4.1	MSE Results . . . . .	B10
4.2	AIR Results . . . . .	B12
5	Conclusions . . . . .	B15
A	Systematic Pilot-Distribution Constructions . . . . .	B15
	References . . . . .	B16

### C Pilot-Aided Joint-Channel Carrier-Phase Estimation in Space-Division Multiplexed Multicore Fiber Transmission **C1**

1	Introduction . . . . .	C3
2	System Model . . . . .	C5

3	CPE Algorithm . . . . .	C7
4	Simulation Results . . . . .	C9
4.1	Comparison Between FGK and BPS for PC-CPE . . . . .	C11
4.2	Power Efficiency . . . . .	C13
4.3	Information Rate . . . . .	C14
4.4	Laser-Linewidth Requirements . . . . .	C16
5	Experimental Results . . . . .	C17
6	Conclusion . . . . .	C21
	References . . . . .	C21

**D On the Performance of Joint-Core Carrier-Phase Estimation in the Presence of Intercore Skew**

**D1**

1	Introduction . . . . .	D3
2	System Model . . . . .	D5
3	CPE Strategy . . . . .	D7
4	Numerical Results . . . . .	D9
5	Discussion and Conclusions . . . . .	D16
A	Derivation of Heuristic Construction . . . . .	D17
	References . . . . .	D18

**E Optimization of Transmitter-Side Signal Rotations in the Presence of Laser Phase Noise**

**E1**

1	Introduction . . . . .	E3
2	System Model . . . . .	E5
3	Proposed Receivers . . . . .	E8
3.1	Joint-Channel Receiver Exploiting Phase-Noise Statistics . . . . .	E8
3.2	Per-Channel Receiver Neglecting Phase-Noise Statistics . . . . .	E9
4	Rotation-Optimization Results . . . . .	E10
4.1	Hadamard Rotations . . . . .	E10
4.2	Optimization Procedure . . . . .	E11
4.3	Results . . . . .	E11
5	Hadamard-Rotation Performance . . . . .	E14
6	Conclusion . . . . .	E17
A	Derivation of Joint-Channel Receiver . . . . .	E18
B	Hadamard-Rotation Asymptotic Analysis . . . . .	E19
	References . . . . .	E21



# **Part I**

# **Overview**



# CHAPTER 1

---

## Background

---

Telecommunications have existed for many centuries and early examples go all the way back to ancient civilizations where information was conveyed using, e.g., smoke signals, mirrors, and drums [1, Pt. 4]. A breakthrough occurred in the 20th century when digital communication systems surfaced and eventually led to a worldwide network called the Internet, which revolutionized the world. The Internet has grown immensely in the last few decades, with the estimated traffic today being more than 20 million times greater than what it was less than three decades ago [2]. Moreover, due to the increasing popularity of modern services such as social media, virtual reality, streaming, and cloud computing, the Internet is still growing at a rapid pace. Fig. 1.1 shows the estimated global Internet traffic per second since 1992 and the predicted rate for 2022.

One of the key enablers of this remarkable growth are fiber-optic communication systems, which today form the Internet backbone due to their enormous throughput capabilities. Broadly speaking, these systems operate by encoding information on light in the near-infrared spectrum and propagating it through an optical fiber. They came into existence in the 1960s with the invention of the laser [3] and optical fiber [4], but worldwide research-and-development efforts did not start until optical fibers with low losses were invented in the 1970s [5]. Since then, the throughput and transmission reach of fiber-optic systems has increased tremendously thanks to a number of technological breakthroughs in the last few decades. This includes the optical amplifier, which was invented in the 1980s [6, 7] and was able to extend transmission reach by up to thousands of kilometers by periodically compensating for the fiber loss. Wavelength-division multiplexing (WDM) [8] was introduced at a similar time and through the simultaneous transmission of multiple wavelength channels, it enabled the utilization of a much broader

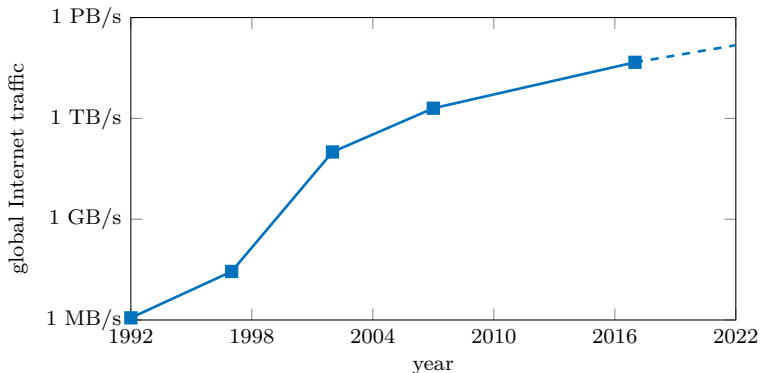


**Figure 1.1:** The estimated global Internet traffic per second over the past decades and a prediction for 2022 [2].

wavelength band in the optical fiber than was previously possible, which dramatically increased the overall system throughput. Moreover, interest in coherent detection was rekindled<sup>1</sup> in the 2000s after it was recognized that together with digital signal processing (DSP), it enabled the use of various algorithms for effective compensation of transmission impairments, as well as the use of advanced modulation formats and polarization-division multiplexing (PDM) [10, 11]. Hence, all available degrees of freedom (amplitude, phase, polarization, and time) of the optical field became available for information encoding, which in turn allowed for higher data rates and transmission distances compared to noncoherent detection.

As seen in Fig. 1.1, the Internet traffic is expected to continue its exponential growth during the next years due to the ever-increasing popularity of bandwidth-hungry Internet-based services. In the past, advances in optical amplification and WDM for systems utilizing single-mode fibers (SMFs) sufficed to support the growth economically, since the amount of data transmitted through the SMF was increased through equipment upgrades [12]. However, as the traffic continues to grow, it is believed that an increasing number of SMFs in optical networks will reach their information-theoretic capacity [13] in the coming years [14]. This is owing to, e.g., amplified spontaneous emission (ASE), launch power restrictions<sup>2</sup>, and optical amplifier bandwidth [16]. Fig. 1.2 shows record throughput demonstrations since 2009 for short-haul transmission over at least 100 km [17–21] and for long-haul transmission over more than 6000 km [22–31]. The current long- and short-haul throughput records stand at 115.9 Tb/s transmission over 100 km [21] and 74.38 Tb/s transmission over 6300 km [31], respectively. As can be seen, the performance

<sup>1</sup>Coherent detection was initially under active research in the 1980s [9], but its development got abandoned soon after due to the success of optical amplifiers and noncoherent WDM-based systems.

<sup>2</sup>Increasing the launch power beyond a certain point degrades the performance of conventional fiber-optic systems and eventually causes fiber fuse, which has catastrophic effects [15].

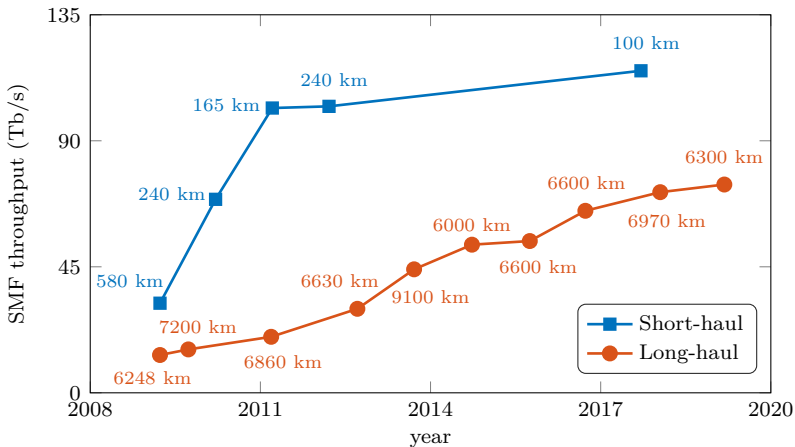


**Figure 1.2:** Record throughput demonstrations over the past decade for short- and long-haul transmission through an SMF. The corresponding transmission distances are marked in the plot.

of state-of-the-art SMF systems in laboratories has only marginally improved since 2011 for short-haul transmission, whereas in the case of long-haul transmission, the maximum demonstrated throughput has seen a linear upwards trend. Unfortunately, it is evident from Fig. 1.1 that the capacity of optical network has to increase exponentially in order to keep up with the Internet-traffic growth. It is conjectured that the only way to achieve this is to add more spatial channels [14], and without technological advances, operators will have to resort to the costly solution of installing new fibers and equipment.

The need for increased capacity along with progress in the development of various fibers and system components [32] has initiated worldwide research efforts for space-division multiplexing (SDM) in recent years, albeit the original concept of SDM dates back to the 1970s [33]. The aim of SDM is to enable cost-effective upscaling of optical networks. This is done through the simultaneous transmission of spatially distinguishable channels together with the integration of system components and the sharing of resources. In particular, since some transmission impairments will be common among the spatial channels in various SDM systems, DSP resources can be shared, which may reduce the computational complexity of algorithms or improve their performance. The concept of sharing DSP resources has also been explored in WDM transmission, e.g., through the use of frequency combs.

In this thesis, we investigate the potential of joint-channel DSP at the transmitter and receiver to mitigate the impact of laser phase noise (LPN) on multichannel transmission. The LPN can be highly correlated over channels in various multichannel systems if lasers are shared by multiple channels. We exploit this fact to assess possible performance improvements for phase-noise compensation (PNC) that can be achieved through joint-channel processing. We consider a simple multichannel phase-noise model that assumes

transmission through of an optical signal through a fiber, followed by receiver DSP that compensates for all impairments except for LPN. Using this model, we develop two high-performance data detection algorithms that perform pilot-aided joint-channel PNC for any number of channels, over which the LPN has arbitrary correlation. Through simulations of coded multichannel transmission, we study their performance in the presence of partially-correlated LPN. The performance of the algorithms is highly dependent on the positions of pilot symbols in time and across channels. Hence, we determine effective pilot distributions for multichannel transmission and assess their performance for various system parameters such as the phase-noise correlation over the channels. Furthermore, in order to verify the validity of the proposed model and algorithms, we use one of the algorithms to process experimental data obtained from uncoded SDM transmission, and compare the results to those predicted by simulations. The system uses an uncoupled, homogeneous, single-mode multicore fiber (MCF), where all cores share the light-source and LO lasers.

Even in the case that lasers are shared for multiple channels, various transmission effects can cause the LPN to become decorrelated across the channels. Propagation delays between channels caused by, e.g., intercore skew in SDM MCF systems or chromatic dispersion (CD) in WDM systems are one of the main causes for such decorrelation. Hence, we propose a multichannel phase-noise model in which intercore skew is accounted for. Using this model, we study the performance of joint-channel PNC in SDM MCF systems that are impacted by intercore skew. In some cases, the LPN may be completely uncorrelated across the channels, even if the lasers are shared by the channels. This scenario typically renders joint-channel DSP for PNC at the receiver unnecessary as it will not improve the performance. Hence, we investigate whether joint-channel DSP at the transmitter can improve the PNC performance instead. In particular, we consider the multichannel transmission of rotated multidimensional signals, where we numerically optimize the rotations using simulations such that the data-detection performance is maximized.

## 1.1 Thesis Organization

This thesis is divided into two parts, where the first part serves as background material for the second part that comprises the publications included in the thesis. The first part is organized as follows. Chapter 2 gives an overview of the building blocks that make up modern fiber-optic communication systems, as well as the main signal impairments that occur during transmission. Chapter 3 describes the typical DSP blocks found in coherent systems, which compensate for the transmission impairments and recover the data. Chapter 4 presents a more detailed background on LPN and presents the multichannel phase-noise model that Papers A–E are based on. Moreover, it reviews the problem of optimal bit detection in the presence of this impairment, as well as different DSP algorithms found in the literature that compensate for LPN in both single-channel and

multichannel transmission. Finally, Chapter 5 summarizes the appended publications and discusses possible directions for future work.

## 1.2 Notation

The introductory part of the thesis uses the following notation conventions. Vectors are denoted by underlined letters  $\underline{x}$ , whereas matrices are expressed by uppercase sans-serif letters  $\mathbf{X}$ . Sets are indicated by calligraphic letters  $\mathcal{X}$ . Boldface letters denote random quantities. The imaginary unit is represented by  $j = \sqrt{-1}$ . The probability of an event is denoted by  $\Pr(\cdot)$ . Moreover, the probability mass function (PMF) of a discrete random variable  $\mathbf{x}$  at  $x$  is written as  $P_{\mathbf{x}}(x)$ , and the probability density function (PDF) of a continuous random variable  $\mathbf{x}$  at  $x$  is denoted by  $p_{\mathbf{x}}(x)$ . The probability distribution of a mixed discrete–continuous random variable is expressed in the same way as PDFs. The Euclidean norm is indicated by  $\|\cdot\|$ , and transposition is denoted by  $(\cdot)^T$ . The number of channels and symbols per transmitted block in each channel are denoted by  $N_{\text{ch}}$  and  $N_s$ , respectively.

There are some notational inconsistencies across the introductory part of the thesis and the appended publications. They are listed here as follows.

- In Papers A–D, the number of symbols per transmitted block in each channel are denoted by  $N$ . Moreover, PDFs and PMFs are denoted by  $p(\cdot)$  and  $P(\cdot)$  in Papers A, C, and D.
- In Paper A, random variables and their realizations are denoted by  $X$  and  $x$ . Scalars, vectors, and matrices are represented by  $x$ ,  $\mathbf{x}$ , and  $\mathbf{X}$ , respectively. The number of channels is denoted by  $D$ . The expectation of a random variable with respect to a distribution  $P$  is written as  $\mathbb{E}_P[\cdot]$ .
- In Papers C and D, notational distinction is not made between random variables and their realizations. Scalars are denoted by  $x$  or  $X$ , vectors are written as  $\mathbf{x}$ , and matrices are represented by  $\mathbf{X}$ . The expectation of a random variable is written as  $\mathbb{E}[\cdot]$ .
- In paper C, the number of cores and channels are denoted by  $D/2$  and  $D$ , respectively, whereas in Paper D, the same quantities are denoted by  $D$  and  $2D$ .
- Papers B and E have the same notational conventions as the introductory part of the thesis, except that the number of channels is denoted by  $M$  and  $N$  in papers B and E, respectively. Moreover, the expectation of a random variable with respect to a distribution  $P$  is written as  $\mathbb{E}_P[\cdot]$  in paper E.



---

## Fiber-Optic Communications

---

The purpose of digital communication systems is to reliably transmit information from one point to another, where the information is in the form of digital messages. Each message is a sequence of bits, which is encoded in the transmitter onto a carrier through a process known as modulation. The carrier propagates through the channel until it reaches the receiver, which attempts to recover the original message. Communication systems that transfer messages using light are commonly referred to as optical communication systems (or lightwave systems) and can further be categorized as guided and unguided systems [34, Ch. 1.3]. Unguided systems are also known as free-space optical communication systems, where a light beam that carries information is propagated unconfined through space, similarly to radio communication systems. These systems are the subject of active research and find their use in both short- and long-range applications, with one of the biggest challenges being the Earth's atmosphere scattering the light beams and significantly degrading the transmission performance [35, Ch. 1.1]. Guided systems, on the other hand, operate by propagating a lightwave carrier in a waveguide and are usually implemented using various types of optical fibers. The cross section of a standard SMF is depicted in Fig. 2.1. The light propagates through a silica core surrounded by a cladding that confines the light to the core during propagation. Outside the cladding is a plastic jacket to protect the fiber, and in some applications, additional sturdier layers are used for further protection. This thesis will focus on fiber-optic communication systems, which are used in many scenarios that require high throughput, e.g., long-haul links forming the Internet backbone or short-haul links for data centers and passive optical networks.

In short-haul applications, the optical link length is on the order of a few meters up to 100 km. Since the installment and maintenance of these links are costly, noncoherent

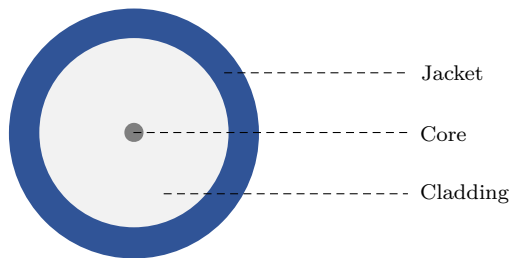


**Figure 2.1:** The cross section of a standard SMF.

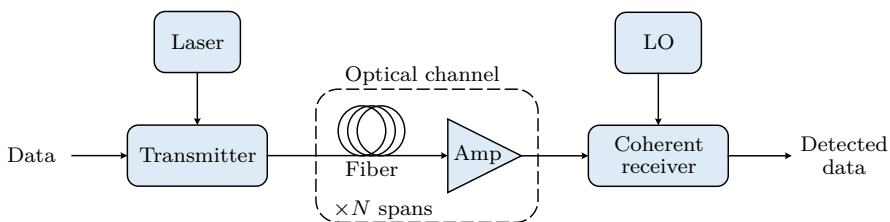


**Figure 2.2:** High-level view of a basic fiber-optic long-haul link consisting of a transmitter,  $N$  spans of an optical fiber and an amplifier, and a coherent receiver.

transmission over multimode fibers (MMFs) has traditionally been the prevalent strategy for economic reasons [36]. On the other hand, coherent SMF systems are capable of higher spectral efficiencies [37] and transmission reaches compared to noncoherent MMF systems, and have thus become the standard for high-performance long-haul links extending to thousands of kilometers. This is due to coherent systems being able to encode information in the amplitude, phase, and polarization of the optical field, whereas noncoherent systems are limited to modulating only the amplitude of the light. In addition, coherent receivers have access to the entire optical field, which enables effective impairment compensation using DSP [10]. The focus in this thesis will be on coherent point-to-point transmission.

## 2.1 Basic System Overview

Fig. 2.2 shows a high-level picture of a basic point-to-point fiber-optic link. The upcoming subsections describe the elements of this system for single-carrier PDM transmission in more details.

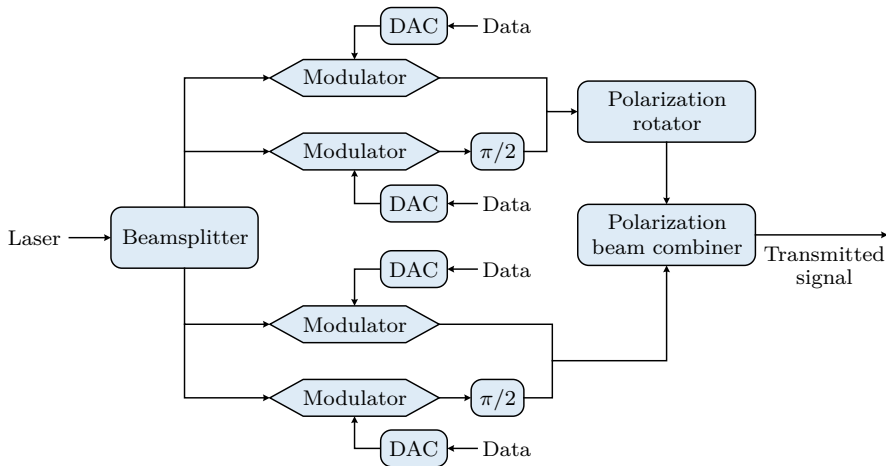


**Figure 2.3:** Overview of a typical optical transmitter for PDM transmission through a single wavelength channel, based on [38, Fig. 3]. (DAC: Digital-to-analog converter)

### 2.1.1 The Transmitter

Fig. 2.3 depicts a typical optical transmitter for single-wavelength, PDM transmission through a standard SMF. A laser that acts as a light source is split into two beams, and each beam enters two modulators that encode information into the in-phase and quadrature components of the lightwave. The electrical signals that represent the data and drive the modulators can be generated in various ways, e.g., through the use of DSP and arbitrary waveform generators. The quadrature component is then phase shifted by  $\pi/2$  and combined with the in-phase component. Both beams are X-polarized at this point, and hence, one of the beams is polarization rotated to become Y-polarized and combined with the other beam through a polarization beam combiner. This results in a four-dimensional PDM signal that is transmitted and propagated through the optical channel, which comprises  $N$  spans, each consisting of an optical amplifier and a fiber span.

### 2.1.2 The Fiber-Optic Channel

A typical fiber-optic link consists of repeated sections called spans, where each span comprises an optical fiber and an optical amplifier. Under certain assumptions, the propagation of a PDM signal through an optical fiber is accurately modeled by the Manakov equation<sup>1</sup> [40]. The Manakov equation is a partial differential equation that describes the propagation of optical complex-baseband signals and accounts for effects

<sup>1</sup>In the case of single-polarization transmission, the signal propagation can be modeled by the nonlinear Schrödinger equation [39, Ch. 2.3].

such as the fiber nonlinearity, CD, and signal attenuation. It is written as

$$\frac{\partial \underline{\mathbf{s}}(z, t)}{\partial z} = -\frac{\alpha}{2} \underline{\mathbf{s}}(z, t) - j \frac{\beta_2}{2} \frac{\partial^2 \underline{\mathbf{s}}(z, t)}{\partial t^2} + j \gamma \frac{8}{9} \|\underline{\mathbf{s}}(z, t)\|^2 \underline{\mathbf{s}}(z, t), \quad (2.1)$$

where  $\|\cdot\|$  denotes the Euclidean norm,  $\alpha$ ,  $\beta_2$ , and  $\gamma$  are the attenuation coefficient, group-velocity-dispersion parameter, and nonlinear coefficient, respectively. The factor  $8/9$  comes due to random birefringence in the fiber. Furthermore,  $\underline{\mathbf{s}}(z, t) = [\mathbf{s}_x(z, t), \mathbf{s}_y(z, t)]$ , where  $\mathbf{s}_x(z, t)$  and  $\mathbf{s}_y(z, t)$  are complex-baseband signals at time  $t$  and location  $z$  propagating in the X and Y polarizations of the optical field. In the right-hand side of (2.1), the first, second, and third terms correspond to fiber loss, CD, and fiber-nonlinearity effects, respectively. The phenomena contained in (2.1), among others, will be described in more details in Section 2.6.

Exact analytical solutions to the nonlinear Schrödinger and Manakov equations have not been found in general, which makes these equations cumbersome for system design and analysis. However, the evolution of  $\underline{\mathbf{s}}(z, t)$  can be obtained numerically using the split-step Fourier method with arbitrary accuracy<sup>2</sup>. Exact analytical solutions can also be found in special cases, e.g., to the nonlinear Schrödinger equation in the case of lossless propagation ( $\alpha = 0$ ) and particular input signals known as solitons [39, Ch. 5].

Simpler models, which approximately describe signals that have propagated through the fiber-optic link and potentially undergone some processing at the receiver are also of interest in order to facilitate system design. In this thesis, we explore such models to design schemes that compensate for LPN in multichannel systems. Naturally, when simplified models are used, it is important to verify the proposed designs through the use of more accurate models or experimental data.

### 2.1.3 The Coherent Receiver

The coherent optical receiver is shown in Fig. 2.4. The received signal and light from the local oscillator (LO) laser are each split into two beams. The beam corresponding to the X-polarization of the received signal enters a  $90^\circ$  optical hybrid along with a laser beam from the LO. These two beams are mixed in a particular fashion to downconvert the received signal. Analogously, the Y-polarized beam of the received signal enters a different  $90^\circ$  optical hybrid with the other LO laser beam, except that it first undergoes polarization rotation to become X-polarized. The outputs from the two hybrids then enter an array of balanced photoreceivers where the in-phase and quadrature components of each polarization are extracted, resulting in four electrical signals. Finally, the signals are sent to an analog-to-digital converter and thereafter to the DSP chain. The DSP chain ends with a demodulator, which outputs either hard decisions or probabilistic information (soft decisions) about the transmitted symbols based on the processed received signal. In the case of coded transmission, this output enters a forward error correction (FEC) decoder, which yields the detected information bits.

<sup>2</sup>Increased accuracy comes at the cost of increased required computational complexity.

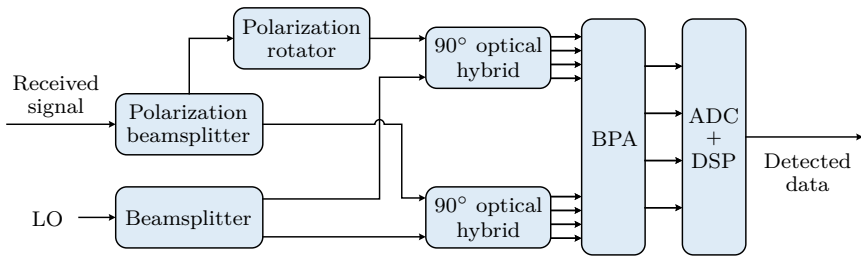


**Figure 2.4:** Overview of the coherent optical receiver for single-wavelength PDM transmission, based on [38, Fig. 4]. (BPA: Balanced photoreceiver array, ADC: Analog-to-digital converter)

## 2.2 Wavelength-Division Multiplexing

Modern optical fibers have a wide spectrum over which it is practical to transmit data due to low losses. The most commonly used band (wavelength range) has traditionally been the C-band, as the fiber has the lowest loss at these wavelengths, but the S- and L-bands also find their use nowadays in research [21, 31] and commercial systems [21]. Together, these bands span 1460–1625 nm and support many THz of bandwidth. However, transmission impairments and hardware limitations put constraints on the maximum symbol rate that can be used in practical systems. Consequently, the available spectrum cannot be utilized by a single carrier [34]. WDM solves this problem by multiplexing many optical carriers at different wavelengths, where each carrier is independently modulated by data and occupies a bandwidth that is manageable by hardware. Modern commercial systems utilizing the C+L bands for transmission carry up to 192 wavelength channels, whereas in laboratory experiments, transmission of several hundred channels has been demonstrated [41].

The channels are separated in frequency by guard bands to prevent interchannel interference and to allow for effective switching in optical networks [41], where the guard bands are typically the order of GHz [42]. Alternatively, WDM with channel spacing as low as the symbol rate of the transmission is also used in order to increase the spectral efficiency of the system. In this case, the channel aggregate is called a spectral superchannel and is transmitted through optical networks as a single entity [43]. Furthermore, the use of frequency combs in WDM superchannel transmission has been extensively researched in recent years [42, 44–46]. Fig. 2.5 depicts a high-level overview of such a system. Frequency combs are sets of equispaced spectral lines and can be used to replace banks of lasers that are normally used as light sources for multiple wavelength channels. As the spectral lines are phase-locked, the resulting LPN will be highly correlated among the wavelength channels [47–49]. This can be exploited to either reduce the DSP complexity or improve system performance in terms of LPN tolerance [47, 50].

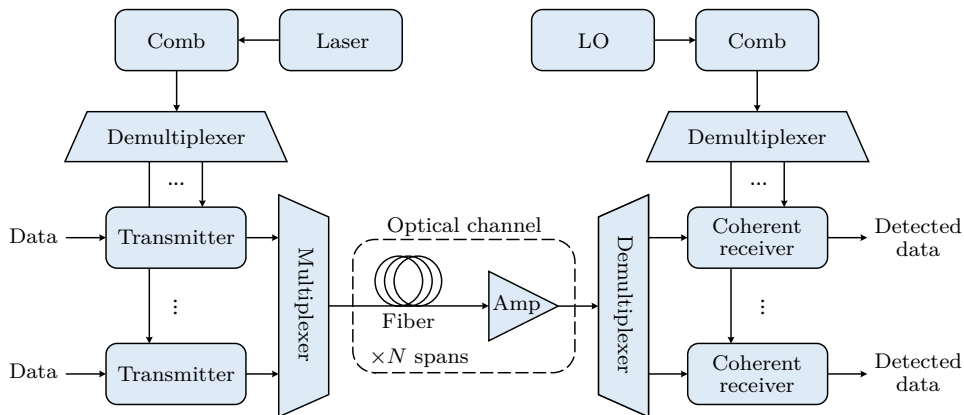


**Figure 2.5:** A high-level overview of a frequency-comb WDM system for transmission of spectral superchannels.

## 2.3 Space-Division Multiplexing

SDM has received a significant research attention in response to the ever-increasing Internet traffic growth. The goal of SDM is to increase the capacity of optical links by transmitting multiple spatial channels in parallel, while keeping the associated cost down. This is done through the integration of system components as well as the use of specialized fibers and amplifiers [51], which leads to the concept of spatial superchannels, i.e., aggregates of multiple same-wavelength spatial channels that are routed as a unity in optical networks [52]. Fig. 2.6 depicts a high-level structure of this type of system, where the SDM multiplexers and demultiplexers are implemented using, e.g., fan-in/fan-out devices [53] or photonic lanterns [54], depending on the type of SDM fiber that is used. Moreover, the optical amplification can be integrated using specialized SDM amplifiers [51, 55]. The rest of this chapter will briefly review different fiber designs that can be used to implement SDM transmission. The cross sections of the considered fibers are illustrated in Fig. 2.7.

### 2.3.1 Bundles of Single-Mode Fibers

The most straightforward approach to realize SDM transmission is to transmit parallel spatial channels over a bundle of multiple SMFs, illustrated in Fig. 2.7 (a). It is simple to implement but has limited potential when it comes to component integration and dense packing of spatial channels [12]. As a consequence, it is not a viable strategy to reduce the cost of upscaling optical networks. However, it is possible to have multiple SMFs share light-source and LO lasers, in which case the LPN will be correlated across the different fibers, which can be exploited [56].

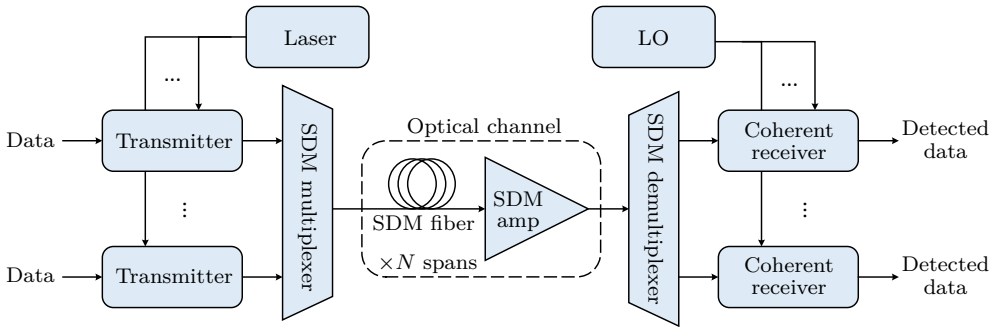


**Figure 2.6:** A high-level overview of an SDM system for transmission of spatial superchannels.

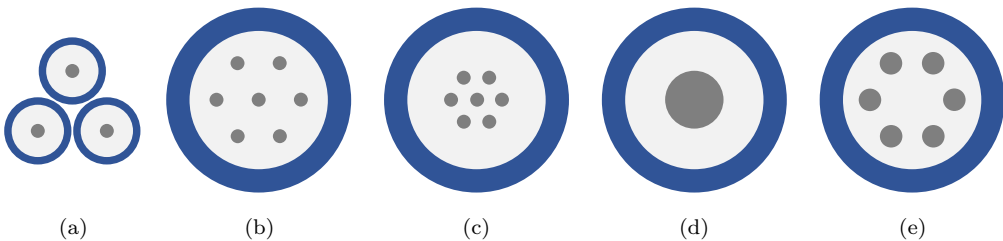


**Figure 2.7:** Fiber designs that can be used for SDM transmission, where (a) is a fiber bundle, (b)–(c) are uncoupled and strongly-coupled MCFs, respectively, (d) is an MMF, and (e) is a multicore–multimode fiber.

### 2.3.2 Multicore Fibers

Fibers where the cladding contains several single-mode cores are called MCFs. The first fabrication of an MCF was reported in the 1970s [33], but it gained limited traction until recently when interest in SDM was revitalized. Today, several types of MCFs are being researched and fabricated worldwide.

Uncoupled-core MCFs are illustrated in Fig. 2.7 (b) and are designed such that the intercore crosstalk, which is mainly governed by the core spacing [57], is minimized. This results in essentially independent parallel spatial channels that are easily separated at the receiver without the need for high-complexity multiple-input multiple-output (MIMO) equalization. A further distinction can be made for uncoupled-core MCFs. In homogeneous fibers, all the cores are engineered to have identical radii and refractive indices, and hence, the same propagation characteristics. As such, the signals propagating through the cores will ideally arrive at similar times<sup>3</sup> at the receiver. This can simplify effective

<sup>3</sup>Due to environmental factors and system imperfections, the signals will typically not arrive simultaneously [58]. This is discussed in more details in Section 2.6.7.

optical switching [56], as well as facilitate various joint DSP and transmission techniques such as self-homodyne detection [59], PNC schemes that reduce DSP complexity [56,60], and multidimensional modulation [61]. In Paper C, we experimentally validate one of the proposed joint-channel PNC algorithms from Paper A using data from transmission through a homogeneous MCF. Furthermore, homogeneous MCFs were used in the record experiments demonstrating the highest throughput of any single-mode MCF (2.15 Pb/s) [62] and the throughput–distance product of any optical fiber ( $4.59 \text{ Eb} \cdot \text{km/s}$ ) [63].

In contrast to the homogeneous variant, the cores in heterogeneous fibers have different radii and refractive indices, which reduces the intercore crosstalk and thus enables a higher number of cores for a fixed core diameter [64]. This is evident from the standing demonstration records for the maximum number of cores, which are 31 and 39 for homogeneous [65] and heterogeneous [66] MCFs, respectively. However, possible disadvantages associated with heterogeneous MCFs are, e.g., higher manufacturing costs and splice losses compared to homogeneous MCFs.

Coupled-core MCFs, illustrated in Fig. 2.7 (c), are designed to have significant intercore crosstalk. This is achieved by spacing the cores closely, which enables a denser packing of spatial channels compared to uncoupled-core MCFs. However, the presence of core coupling and intercore skew results in signal dispersion and mixing during propagation through the cores, which requires high-complexity MIMO equalization at the receiver, analogous to polarization demultiplexing in the case of PDM transmission. Hence, coupled-core MCFs are typically engineered to minimize dispersion in order to reduce the required equalization complexity [67].

### 2.3.3 Multimode Fibers

The concept of MMFs was originally proposed decades ago, with the first fabrication reported in the 1970s [68]. In contrast to MCFs, MMFs have only one core within the cladding as illustrated in Fig. 2.7 (d), but the core diameter is wide enough to allow for the propagation of multiple modes. MMFs have traditionally been used for noncoherent transmission in cost-constrained applications such as short-haul links in optical networks. For coherent SDM transmission, however, MIMO equalization becomes necessary at the receiver due to mode coupling and modal dispersion. Despite this, it has been shown that MMFs can simplify the upscaling of optical-network switches [69] and reduce nonlinearities [70]. As a result, MMFs have been studied extensively in recent years for SDM applications, in which case they are often referred to as few-mode fibers. This is because they are designed to support a limited number of modes, with 45 being the highest demonstrated number of modes in transmission thus far [71]. Moreover, high phase-noise correlation among the modes has been demonstrated in MMF transmission, enabling the use of PNC schemes that reduce the DSP complexity [72,73].

### 2.3.4 Multicore–Multimode Fibers

In addition to plain MCFs and MMFs, fibers using combinations of multiple cores and modes have been fabricated and studied, where many multimode cores are located within the same cladding as depicted in Fig. 2.7 (e). This type of fiber holds the record for the highest number of spatial channels supported by a single fiber, where PDM transmission through a 3-mode 39-core fiber was demonstrated in [66]. In this demonstration, one core was reserved for pilot-tone transmission enabling the use of low-complexity DSP, whereas the other 38 cores were used for data transmission, resulting in a total of 228 spatial channels (including polarizations). Furthermore, a multimode–multicore fiber was used in a record-breaking experiment achieving the highest demonstrated throughput of any fiber (10.16 Pb/s) [74]. This was achieved through transmission of a total of 84 246 WDM and SDM channels.

## 2.4 Modulation Formats

In the transmitter, electrical signals are used to encode information onto the amplitude and phase (or analogously, the in-phase and quadrature components) of each optical-carrier polarization, where the electrical signals represent the bit sequence to be transmitted. This step is part of a process called modulation, in which a bit sequence is encoded onto an optical carrier. First, groups of bits are mapped to symbols, which are traditionally defined as scalar complex points<sup>4</sup>. The symbol sequence is then converted to an analog waveform comprising a train of pulses. Mathematically, this is written as

$$\mathbf{s}(t) = \sum_{k=1}^{N_s} \mathbf{s}_k p(t - kT_s), \quad (2.2)$$

where  $\mathbf{s}_k$  is the  $k$ th elements in the symbol sequence of length  $N_s$ ,  $p(t)$  is a real-valued pulse, and  $T_s$  is the symbol interval. Common choices of  $p(t)$  are raised-cosine and root-raised-cosine pulses [37, 78]. Finally, the real and imaginary parts of the waveform in (2.2) form the electrical signals that drive the modulators for each polarization in the transmitter depicted in Fig. 2.3.

The symbols take on values from a set of constellation points,  $\mathcal{X}$ , called a modulation format. The constellation points in this set are typically zero mean and have variance  $E_s$ . Common modulation formats in fiber-optic communications nowadays are PDM phase-shift keying (PSK) and PDM quadrature amplitude modulation (QAM), where PDM refers to the same format being used in both polarizations of the optical carrier. In general, increasing the number of points in  $\mathcal{X}$  translates to a higher spectral efficiency, since each constellation point represents an increased number of bits. This comes at the cost of an increased sensitivity to distortions in the received signal after transmission.

<sup>4</sup>Symbols are sometimes defined as multidimensional points, e.g., when modulation is performed jointly over polarizations, frequency, space, or time [61, 75–77].

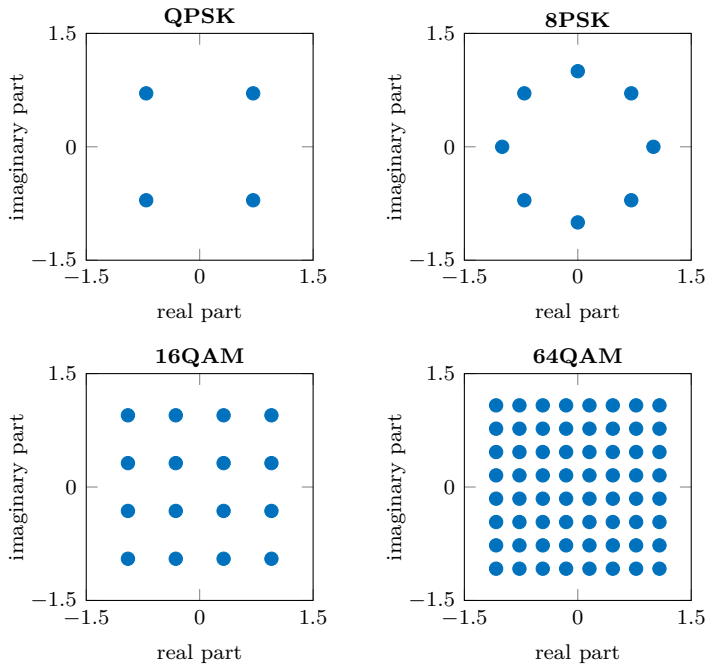


**Figure 2.8:** Illustration of different PSK and QAM formats with  $E_s = 1$ .

Fig. 2.8 exemplifies QPSK (also known as 4PSK or 4QAM), 8PSK, 16QAM, and 64QAM. Assuming that all constellation points are selected with equal probability, these formats carry  $\log_2 M$  number of bits, where  $M$  is the number of constellation points. More advanced higher-order and multidimensional formats have also been used in recent years. Transmission of PDM-16384QAM has been demonstrated [79], carrying 22.3 information bits per four-dimensional symbol, whereas optimized joint modulation in 4, 8, and 24 dimensions has been shown to improve system performance [75, 76, 80, 81], particularly in terms of nonlinearity resistance [82].

A related topic is constellation shaping, which has its origins in information theory established by Shannon [13]. Every practical channel distorts the transmitted signal, typically in a stochastic manner, introducing errors in the data detection. In fact, all practical channels are fundamentally limited in how much information they can carry such that the data can be detected with arbitrarily low error probability. This limit is called the channel capacity, and Shannon showed that this limit can be approached by using error correcting codes of large lengths, provided that the signal has a capacity-achieving distribution. Constellation shaping is motivated by the well-known fact that Gaussian signaling has a capacity-achieving distribution for the additive white Gaussian noise (AWGN) channel, which is infeasible to implement in real systems. However, the use of more practical modulation schemes with equiprobable constellation points introduces

a shaping gap, meaning that the channel capacity cannot be approached due to the use of suboptimal modulation formats.

Shaping involves approximating the capacity-achieving distribution using a practical implementation. Thanks to advances in hardware and methods to implement shaping, this topic has in recent years gained significant traction in fiber-optic communications, although the original concept dates back to the 1980s [83]. A fiber-optic link is not a simple AWGN channel, and its capacity is in fact still not exactly known [16]. Nevertheless, the benefits of shaping have been experimentally demonstrated in various systems [79, 84–88]. The two main categories of shaping are geometric and probabilistic shaping. The former involves constellations with nonuniformly spaced but equiprobable points, whereas the latter entails placing constellation points with varying probabilities on a fixed grid (typically using square QAM formats as templates).

## 2.5 Forward Error Correction

The basic principle of error control coding is to add systematic redundancies to information bit sequences on the transmitter side, which can be exploited on the receiver side in order to cope with more signal distortion when performing data detection. In practical systems, the application of error control coding involves using effective codes that allow for operation closer to the channel capacity compared to uncoded transmission given constraints on, e.g., latency and power consumption. In high-rate and long-haul transmission, retransmission is considered impractical as it can cause large delays due to the extreme transmission distances. Consequently, error correction is usually performed solely at the receiver without the use of retransmission schemes [12], and hence, it is typically referred to as FEC in fiber-optic communications. Due to the absence of retransmission schemes, reliability requirements are typically quite stringent, where data bit error rates (BERs) of down to  $10^{-15}$  are required [89].

Historically, Hamming and Reed–Solomon codes were used to satisfy reliability requirements in fiber-optic communications [12]. In recent years, however, low-density parity-check (LDPC) [90] codes, turbo codes [91], and polar codes [92] have seen an increase in popularity. In particular, the use of binary FEC codes in conjunction with bit-to-symbol mapping, referred to as coded modulation [93], is a common technique nowadays. It allows systems to operate at higher effective data rates and transmission distances than what would be possible in uncoded transmission [93]. Moreover, the iterative nature of LDPC and turbo decoders allows for cooperation between the decoder and impairment-compensation or detection schemes [94–99]. We use this technique in Paper A for the compensation of LPN in the context of coded multichannel fiber-optic transmission. Furthermore, depending on the code, either soft-decision or hard-decision decoding can be performed, where the latter has less computational complexity at the cost of degraded performance compared to the former [89].

Most FEC codes that are used in fiber-optic communications are designed for the

time-discrete AWGN channel, which is in general not an accurate description of the fiber-optic channel. However, after the received signal has undergone DSP in the receiver, the noise in the processed time-discrete signal is in many realistic transmission scenarios well approximated as AWGN [100]. This justifies the use of codes designed for the AWGN channel and explains their effectiveness in fiber-optic communications.

## 2.6 Transmission Impairments

Although this thesis is focused on the compensation of LPN, other impairments cannot be ignored as they will affect the performance of PNC. This section gives an overview of the main transmission impairments that occur due to physical properties of the fiber-optic channel and imperfections in various hardware components.

### 2.6.1 Additive Noise

The silica core in modern optical fibers through which the lightwave propagates is remarkably transparent. It was introduced in 1979 [101] and was one of the inventions that initiated the rapid progress of fiber-optic communication systems in the coming decades. However, despite its transparency, the silica core exhibits a wavelength-dependent transmission loss, with a minimum loss of approximately 0.2 dB/km for wavelengths at around 1550 nm. This loss becomes significant in long-haul transmission and has to be compensated; otherwise, the signal will be undetectable at the receiver. Initially, to overcome this problem, optoelectronic regenerators were placed at regular intervals in the optical link that detected and retransmitted the data, but as they had similar costs as typical pairs of endpoint transceivers [102], this solution became expensive and complex for WDM systems. Moreover, regenerators are incompatible with elastic optical networking [103] as they must be configured for a fixed combination of, e.g., baud rate, modulation format, pulse shape, and WDM grid.

In the 1980s, a more economical and flexible way of compensating for the loss was proposed where the optical signal could be amplified simultaneously at multiple wavelengths without the need for detection and retransmission, using an optical amplifier such as the erbium-doped fiber amplifier [6, 7] or the Raman amplifier [104]. However, the amplification is accompanied by amplified spontaneous emission, which manifests as additive noise in the transmitted signal. This degrades the performance of DSP algorithms and, more importantly, puts a fundamental limitation on the possible transmission reach [105].

### 2.6.2 Polarization Effects

As previously mentioned, coherent fiber-optic systems exploit the fact that light has two orthogonal polarization states that can be encoded with data independently. This orthogonality is preserved as the signal propagates if the optical fiber has a perfectly

cylindrical core. In reality, however, the shape of the core will vary along the fiber due to imperfections in the manufacturing process as well as mechanical and thermal stress, causing the fiber to have a random birefringence<sup>5</sup> [39, Ch. 1.2]. As a consequence, the polarization state of the light rotates randomly during propagation, leading to polarization coupling. Moreover, due to the fiber birefringence, the two polarizations will propagate at different velocities in the fiber, resulting in a phenomenon called polarization-mode dispersion (PMD) that manifests as pulse broadening [39, Ch. 2.2]. Finally, polarization-dependent loss (PDL), typically defined as the ratio between the maximum and minimum polarization-dependent power gains with respect to all possible polarization states [106], is an effect that originates in various optical components [107] and can lower the signal-to-noise ratio (SNR) and orthogonality between the polarizations [108].

### 2.6.3 Chromatic Dispersion

The optical fiber has a wavelength-dependent refractive index, which originates from a property of the fiber material called CD. Due to this, the different spectral components of the signal travel at different velocities through the fiber [39, Ch. 1.2]. This effect can be regarded as an all-pass filter, i.e., a filter that applies a frequency-dependent phase shift to the signal while leaving its amplitude unaffected. It causes a deterministic pulse broadening that increases with the length of the optical link and severely limits the transmission reach of fiber-optic systems if left uncompensated. However, the amount and characteristic of the CD also depend on a dispersion parameter that can be controlled in the fiber design process. As a result, the pulse broadening can be reduced through the use of dispersion-shifted fibers that have minimum dispersion at the carrier wavelength or completely reverted by adding so-called dispersion-compensating fibers to optical links in addition to the standard fibers.

### 2.6.4 Nonlinearities

In addition to being wavelength dependent, the refractive index of the optical fiber changes in proportion to the light intensity. This phenomenon is called the optical Kerr effect and is the cause of various nonlinear signal effects that occur during propagation, such as self-phase modulation (SPM), cross-phase modulation (XPM), and four-wave mixing (FWM) [39, Ch. 2.6]. These effects degrade the performance of conventional fiber-optic systems if the launch power on the transmitter side is increased beyond a certain point. SPM entails an optical pulse inducing a nonlinear phase shift to itself proportional to its intensity and the optical link length, which also leads to spectral broadening [39, Ch. 4]. XPM occurs during simultaneous transmission of multiple channels, e.g., PDM or WDM signals. Its manifestation is similar to SPM, but the nonlinear phase

---

<sup>5</sup>Birefringence is a property of the fiber material entailing a refractive-index dependence on the polarization of the light.

shift of a pulse is proportional to the light intensity of copropagating pulses<sup>6</sup> [39, Ch. 7]. FWM is a phenomenon where three copropagating frequency components generate a fourth component with a particular frequency. This leads to interchannel interference and can degrade the performance of WDM systems [34, Ch. 2.3]. Moreover, due to the Kerr effect, light propagating through the fiber produces nonlinear birefringence whose magnitude is dependent on the state of polarization and intensity of the light. This leads to a self-induced change in the light's state of polarization, referred to as nonlinear polarization rotation [39, Ch. 6.1].

The aforementioned impairments pertain to signal–signal interactions. Hence, they are deterministic and can be compensated for in the optical domain [109, 110] or in DSP [111, 112]. However, the interplay between ASE and Kerr nonlinearities gives rise to signal–noise and noise–noise interactions, which lead to stochastic impairments such as nonlinear phase noise that fundamentally limit the transmission performance [16].

Another nonlinear effect pertaining to optical fibers is electrostriction, where light intensity causes the fiber material to become compressed. This effect leads to a process called stimulated Brillouin scattering that puts a limit on the possible launch power [34, Ch. 2.6]. A related process is stimulated Raman scattering, which can negatively affect WDM systems even for modest launch powers. However, it can also be exploited to amplify optical signals, in which case it is known as Raman amplification [104].

### 2.6.5 Carrier-Frequency Offset and Laser Phase Noise

The coherent receiver in modern systems performs so-called intradyne detection [113], where an LO is mixed with the received signal to extract the in-phase and quadrature components from the polarizations. The LO is tuned to approximately match the frequency of the received carrier wave. However, it is not phase locked to the carrier, which causes a frequency and phase mismatch between the LO and the received signal. This manifests as a linear phase rotation of the received samples after analog-to-digital conversion.

Since coherent systems typically encode information in the amplitude and phase of the light, lasers used for fiber-optic communications should ideally be able to produce a perfect sinusoidal carrier wave. In other words, the optical spectrum of the laser output should be a delta function. In reality, however, this is not the case as there will be phase fluctuations in the optical field produced by the laser [114, Ch. 7.6]. The fluctuations are statistically independent of each other as they come due to spontaneous emission in the laser. They cumulatively perturb the carrier phase, which gives rise to a process that drifts with time and is called LPN. Each symbol in modulated transmission experiences the accumulation of many such phase fluctuations, which will be approximately Gaussian distributed due to the central limit theorem [115, Ch. 3.1]. As a consequence, LPN is

---

<sup>6</sup>XPM-induced phase shifts can be approximated as random walks in the case of WDM transmission with ideal distributed Raman amplification [99].

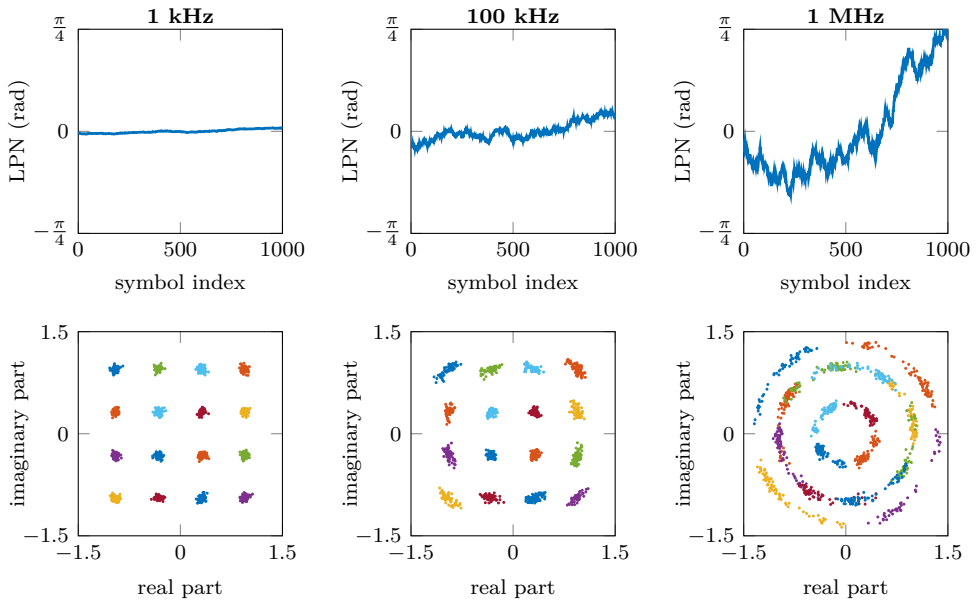


**Figure 2.9:** Top: Realization of the LPN random-walk model for 20 GBd transmission and different laser linewidths. Bottom: The impact of the LPN depicted in the top plots on transmitted 16QAM symbols.

typically modeled as a Gaussian random walk, i.e., a discrete process given by

$$\boldsymbol{\theta}_k = \boldsymbol{\theta}_{k-1} + \Delta\boldsymbol{\theta}_k, \quad (2.3)$$

where  $\boldsymbol{\theta}_k$  is the LPN at time index  $k$  and  $\Delta\boldsymbol{\theta}_k$  is a Gaussian random variable with zero mean and variance  $2\pi\Delta\nu T_s$ . The parameter  $T_s$  is the inverse of the transmission baud rate [115, Ch. 2.5] and  $\Delta\nu$  is the combined laser linewidth [116] of the light-source laser at the transmitter and the LO laser at the receiver<sup>7</sup>. Laser linewidths encountered in the literature range from a few kHz [118] up to several MHz [119], but are most commonly on the order of 100 kHz. Each  $\boldsymbol{\theta}_k$  manifests as the  $2\pi$ -periodic rotation  $e^{j\boldsymbol{\theta}_k}$  in the complex-valued signal space, and hence, the LPN inherently has a  $2\pi$  ambiguity. The initial condition of (2.3),  $\boldsymbol{\theta}_0$ , is typically set to zero or distributed uniformly in the range  $[0, 2\pi)$ . Fig. 2.9 exemplifies realizations of (2.3) across 1000 symbols and the resulting impact on 16QAM transmission at 20 GBd for different laser linewidths.

<sup>7</sup>The phase noise of real lasers does not behave exactly as a random walk [114, Ch. 7.6]. Moreover, due to CD, the observed LPN at the receiver is not simply the sum of phase noise produced by the light-source laser and the LO laser [117]. Nevertheless, (2.3) is the prevailing LPN model used in the literature.

### 2.6.6 I/Q Imbalance

As mentioned earlier, in coherent communication systems, information is encoded in the amplitude and phase, i.e., in the orthogonal in-phase and quadrature components of the carrier wave. However, imperfections in the transceiver hardware lead to phase and amplitude errors in the components, causing them to lose orthogonality. This phenomenon is referred to as I/Q imbalance, and its origins on the transmitter side are, e.g., incorrect bias-points settings and imperfect splitting ratio of couplers [120]. On the receiver side, further amplitude and phase errors in the received signal can be caused due to imperfections in the  $90^\circ$  optical hybrids and balanced photodiodes [121].

### 2.6.7 Propagation Delays between Channels

In multichannel transmission, environmental conditions [122] and properties of the fiber can lead to relative propagation delays between channels. This is observed in WDM systems where the fiber has a wavelength-dependent refractive index due to CD, causing the wavelength channels to propagate at different velocities [45]. Moreover, in SDM transmission using MCFs, differences in the refractive index between the cores cause the signals to propagate at core-dependent velocities, leading to intercore skew [58]. This effect is particularly pronounced in heterogeneous MCFs, where the cores are intentionally made to have different refractive indices [64]. However, it is also observed in homogeneous MCFs, which are manufactured to have identical refractive indices among the cores, but imperfections lead to slight differences that cause intercore skew up to hundreds of ps/km [123].

Although typically not a limiting factor in transmission where each channel is modulated and processed independently, propagation delays between channels can impact joint processing. Particularly in the case that light-source and LO lasers are shared among channels, the light-source LPN in each channel will mix with the LO LPN at different times due to the relative delays, which is illustrated in Fig. 2.10. This can be detrimental to the performance of joint-channel DSP schemes that exploit this correlation [58, 60]. In Paper D, we investigate the effects of intercore skew on the joint-core compensation of PNC.

## 2.7 Performance Metrics

There are various ways to assess the performance of systems. In communications, the metrics of interest are usually related to how much information can be conveyed over the channel given a reliability (error rate) criterion. Other metrics can also be useful for gaining insight during the design of DSP algorithms. This section explains the main performance metrics used in fiber-optic communications nowadays, particularly for transmission in the presence of LPN.

The mean squared error (MSE) is used to assess the accuracy of parameter estimates.

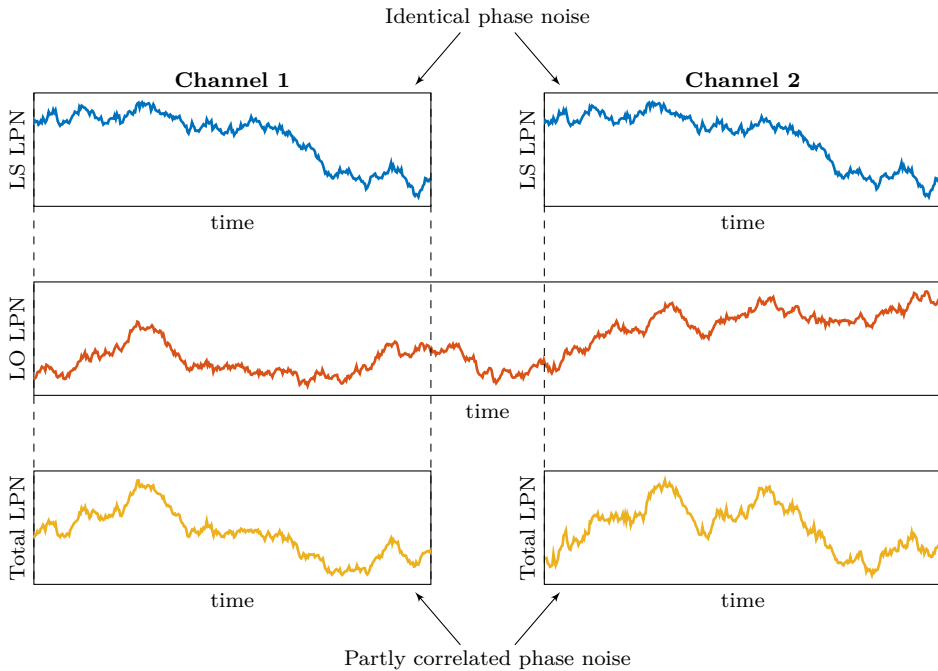


**Figure 2.10:** Illustration of 2-channel transmission where the light-source and LO lasers are shared among the channels, but due to relative propagation delays, the combined LPN is only partly correlated between the channels.

It does so by computing the average squared error, where the error is the difference between the estimate and the ground truth. Mathematically, this is written as

$$\text{MSE} = \frac{1}{N} \sum_{i=1}^N (\hat{\theta}_i - \theta_i)^2, \quad (2.4)$$

where  $\hat{\theta}_i$  and  $\theta_i$  are the estimates and ground truth, respectively, and  $N$  is the number of samples. This metric is frequently used in the context of PNC [124–127]. Note that if  $\theta_1, \dots, \theta_N$  are realizations of LPN, the phase error is more appropriately computed as  $\arg\{e^{j(\hat{\theta}_i - \theta_i)}\}$  instead of  $(\hat{\theta}_i - \theta_i)$ , since phase is invariant under any  $\ell 2\pi$  rotation where  $\ell$  is an integer.

Detection error probability is a common metric in communications to measure the reliability of a system. The most common metrics that approximate error probabilities encountered in fiber-optic communications are BERs, symbol error rates (SERs), and block error rates (BLERs). BER corresponds to the probability that the detector makes

the wrong bit decision, i.e.,

$$\Pr(\text{wrong bit decision}) = \sum_{b \in \{0,1\}} \Pr(\hat{\mathbf{b}} \neq b | \mathbf{b} = b) P_{\mathbf{b}}(b), \quad (2.5)$$

where  $\hat{\mathbf{b}}$  and  $\mathbf{b}$  are the detected and transmitted bit, respectively. Analogously, SER and BLER correspond to the probability of symbol-wise and symbol-block-wise decision errors, respectively.

BER is typically classified in fiber-optic communications into pre- and post-FEC BER, pertaining to the detection error probability of coded and information bits, respectively. Error probabilities are often difficult to compute analytically but can be estimated numerically through Monte Carlo simulations. In general, the lower the error probability, the harder it is to numerically estimate it with a reasonable accuracy, and since targeted post-FEC BERs are often as low as  $10^{-15}$ , they are infeasible to estimate. Due to this, pre-FEC BERs have up until a few years ago been estimated and used to predict the post-FEC BER performance of the system for hard- and soft-decision decoding schemes [19, 128, 129].

Pre-FEC BERs are effective for hard-decision decoding that takes as inputs the detected coded bits. However, in the case of soft-decision decoding, achievable information rates (AIRs) are found to be more accurate predictors of the post-FEC BER performance. AIRs determine how much information can be conveyed over a channel with an arbitrarily low error rate, assuming the use of a capacity-achieving FEC code with ideal decoding [93]. Mutual information (MI) or generalized mutual information (GMI)<sup>8</sup> are typically the AIRs of choice in fiber-optic communications, depending on the type of coded-modulation scheme used. In particular, when coded modulation based on binary FEC codes with soft-decision decoding is used, which is arguably the most common setup nowadays, GMI is the most prevalent metric in the literature. It is defined as the AIR for a bit-wise decoder and its mathematical expression depends on the channel model. Typically, the complex AWGN channel is assumed for symbol detection, in which case the GMI can be estimated through Monte Carlo simulations [93, Eq. 35] as

$$\text{GMI} \approx m - \frac{1}{N_s} \min_{s \geq 0} \sum_{k=1}^m \sum_{i=1}^{N_s} \log_2 \left( 1 + e^{s(-1)^{c_{k,i}} \gamma_{k,i}} \right) \quad (2.6)$$

where  $m$  is the number of bits per symbol,  $N_s$  is the number of transmitted symbols,  $c_{k,i}$  is the  $k$ th coded bit associated with the  $i$ th symbol, and  $\gamma_{k,i}$  is the log-likelihood ratio (LLR)<sup>9</sup> of  $c_{k,i}$ . Skipping the minimization in (4.3) and setting  $s = 1$  can be done if the actual channel over which is transmitted is the complex AWGN channel and the LLRs are computed exactly. Otherwise, doing this will yield an AIR which is lower than the GMI [93].

<sup>8</sup>In the case that probabilistic shaping is used, a variant of the GMI called the normalized GMI [130], as well as a metric referred to as asymmetric information [131], have been shown to be more effective than the GMI.

<sup>9</sup>LLRs represent soft information about the coded bits and are the inputs to soft-decision decoders.

In this section, some of the main DSP techniques used in modern fiber-optic systems will be discussed. In particular, a typical DSP chain that is used in the coherent receiver is detailed.

### **3.1 Transmitter DSP**

The majority of DSP is in most cases performed on the receiver side in fiber-optic transmission. However, there is a number of DSP steps that are typically applied in the transmitter, such as pulse shaping [31] where symbol sequences are mapped to the waveforms that yield the electrical signals driving the modulators (see Fig. 2.3). Dispersion precompensation and precoding can be performed prior to transmission [78, 132, 133], which is particularly useful in direct-detection systems. Precompensation of nonlinearities in various systems has also been studied [134–136]. In particular, it has been shown that combining pre- and postcompensation of nonlinearities can yield better results than when pre- or postcompensation is performed alone [137, 138]. PDL mitigation has also been proposed through the use of space–time coding [139–141]. Space–time coding has been used to, e.g., mitigate more-dependent loss (MDL) in SDM MMF transmission [142], improve tolerance to interchannel interference [143] in WDM transmission, and reduce the impact of nonlinearities [141]. Moreover, the use of orthogonal or unitary signal transforms has been studied to improve performance in WDM systems by equalizing distortions over the channels [144], as well as to mitigate PDL and MDL [145, 146]. In Paper E, we study the use of such transforms, namely rotations, for multichannel transmission

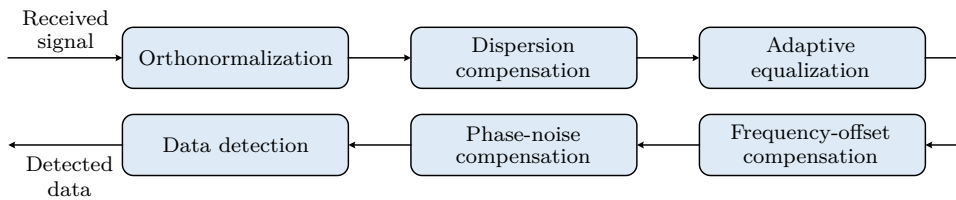


**Figure 3.1:** A basic DSP chain used in the coherent receiver.

in the presence of LPN.

## 3.2 Receiver DSP

Fig. 3.1 depicts a basic DSP chain in the coherent receiver required to compensate for the impairments discussed in Section 2.6 and detect the transmitted data. The ordering of the steps in Fig. 3.1 is not unique, and the chain does not include all possible techniques that are performed in the coherent receiver, such as deskewing [147], timing recovery [148], and fiber nonlinearity mitigation [149]. The rest of this section reviews algorithms from the literature to implement all the steps in Fig. 3.1 except for PNC, which will be the focus of Chapter 4. DSP for multichannel transmission such as high-order MIMO equalization [71, 150] will not be covered. Instead, this section focuses on methods that are used in standard SMF transmission. These methods can be used on a per-channel basis for some multichannel systems. Indeed, this was the case for the MCF experimental setup used for Paper C, where all DSP stages except PNC were applied separately on each core.

### 3.2.1 Orthonormalization

As discussed in Section 2.6.6, I/Q imbalance decreases the orthogonality between the in-phase and quadrature components of a signal. This can be compensated through a process called orthogonalization, and if accompanied with signal normalization to correct for amplitude errors, it is referred to as orthonormalization. Typically, the Gram–Schmidt algorithm is used to achieve this. It was originally developed in the field of mathematics to construct an orthogonal basis from an arbitrary one, and eventually it was utilized to compensate for I/Q imbalance in the context of fiber-optic communications [120]. However, this method increases the impact of quantization noise in one of the signal components. Alternatively, the Löwdin algorithm can be used, which constructs a set of symmetrically orthogonalized components that are closest to the original components in the least mean-squares sense [151]. As a result, the impact of quantization noise is distributed equally in the two components [152]. Other solutions have been proposed specifically for transmission of quadrature phase-shift keying (QPSK) [153–155].

At this stage in the DSP chain, I/Q imbalance that originates in the transmitter cannot be directly compensated due to the presence of other impairments, such as carrier-frequency offsets and phase noise. Instead, a second orthonormalization step can be performed after PNC. Joint estimation of phase noise and transmitter I/Q imbalances has also been proposed [156].

### 3.2.2 Dispersion Compensation

CD can be regarded as an all-pass filter with the transfer function [157]

$$G(f) = \exp\left(-j\frac{\pi f^2 \lambda^2 D}{c}\right), \quad (3.1)$$

where  $c$  is the speed of light,  $\lambda$  is the carrier wavelength,  $D$  is the dispersion parameter, and  $f$  is frequency. Since CD affects the two polarizations of the light identically, it can be compensated through static equalization using identical filters for each polarization with the transfer function  $1/G(f)$  [158]. The filtering can be done in the frequency domain, but practical implementations are usually carried out in the time domain using finite impulse response (FIR) or infinite impulse response filters [10, 158–160].

In practical systems, the exact accumulated dispersion is not known even if the dispersion parameters specified for the optical fibers in the link are given. However, multiple blind methods that operate without prior knowledge of the transmitted data have been proposed to estimate the accumulated dispersion [157, 161–163]. Alternatively, pilot-aided methods<sup>1</sup> that utilize signals known to the receiver can be used [164, 165].

### 3.2.3 Adaptive Equalization

While static equalization may compensate for CD, polarization-dependent impairments such as PMD and polarization rotation/coupling are dynamic processes that require adaptive equalization to be undone. Typically, this is carried out at two samples per symbol using a MIMO equalizer that consists of four complex-valued FIR filters connecting the inputs and outputs through a butterfly structure [152]. This structure is illustrated in Fig. 3.2, where at each time  $k$ , the inputs are windows of received samples around the  $k$ th sample, denoted with  $\mathbf{r}_{x,k}^{\text{in}}$  and  $\mathbf{r}_{y,k}^{\text{in}}$ , and the outputs are equalized samples, denoted with  $\mathbf{r}_{x,k}^{\text{out}}$  and  $\mathbf{r}_{y,k}^{\text{out}}$ . Moreover, the four FIR filters are denoted as  $\underline{h}_{xx}$ ,  $\underline{h}_{xy}$ ,  $\underline{h}_{yx}$ , and  $\underline{h}_{yy}$ . The purpose of the equalizer is to reverse the polarization coupling, i.e., demultiplex the polarizations, as well as to mitigate PMD. However, the equalizer also approximates the matched filter and compensates to some extent timing errors and residual CD. To accomplish the adaptive equalization, the filter taps are updated recursively by minimizing a cost function through an update algorithm such as stochastic gradient descent until convergence is reached. However, even after

<sup>1</sup>Blind and pilot-aided methods are also called non-data-aided and data-aided methods, respectively.

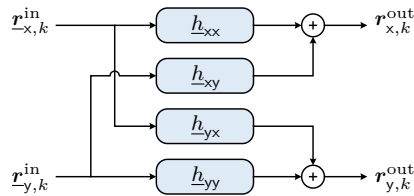


**Figure 3.2:** Illustration of the adaptive equalizer, entailing four FIR filters and a particular connection between the inputs and the outputs.

convergence, there is no guarantee that the equalizer manages to compensate properly for the aforementioned impairments. The equalization performance depends on the cost function, the filter-tap initialization, and the parameter setting pertaining to the update algorithm.

Several blind equalizers have been proposed in the literature, differing mainly in the cost function used to update the filter taps. The constant modulus algorithm (CMA) [166] is a blind equalizer that relies on the transmitted symbols having constant amplitude, which is the case for PSK modulation formats. For multimodulus formats such as higher-order QAM, the CMA has suboptimal convergence and steady-state performance as the constant-modulus criterion is not fulfilled [167]. In this case, other variants are more effective, such as the radially-directed equalizer, also known as the multimodulus algorithm [168], and decision-directed equalizers [169]. Alternatively, a trained equalizer [152] using a sequence of transmitted pilot symbols known to the receiver can be used to achieve equalization with high accuracy. Finally, it is worth noting that the CMA is routinely used for pre-convergence of the filter taps, followed by the operation of some of the other aforementioned equalizers, as this is found to improve the overall equalization performance [169].

### 3.2.4 Frequency-Offset Compensation

While compensating for frequency offsets and LPN can be done jointly, these steps have traditionally been separated in DSP, and hence, the linear phase rotations caused by frequency offsets in the receiver are mitigated prior to PNC. Numerous blind algorithms have been proposed for frequency-offset estimation. A differential phase-based method can be used where the maximum likelihood estimate of the frequency offset is obtained [170]. A similar method was proposed in [171], but it performs the estimation recursively. Spectral methods can also be used, where the received samples are preprocessed (typically raised to the fourth power) and then Fourier transformed, which allows searching for a peak in the spectrum corresponding to the frequency offset [172]. An iterative method based on this concept was proposed in [173], improving upon the estimation accuracy and effectiveness for higher-order QAM. Various other blind and pilot-aided algorithms

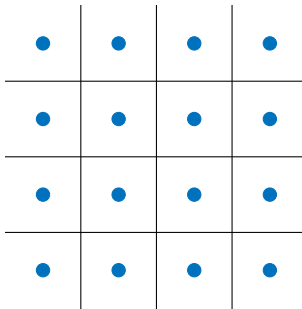


**Figure 3.3:** A decision-region illustration of the minimum-Euclidean-distance symbol detector for 16QAM in the case of equiprobable symbols, where the dots and lines correspond to constellation points and edges of the decision regions, respectively.

exist and are reviewed in [172].

### 3.2.5 Data Detection

After all impairments have been compensated, data detection is performed, which is the process of recovering the data-bit sequence that was conveyed over the optical channel. For uncoded transmission, data detection is typically carried out through symbol detection followed by a demapper, which maps the detected symbols to bits. The maximum *a posteriori* (MAP) symbol detector is optimal in the sense that it yields minimum SER. For the AWGN channel and equiprobable symbols, this detector operates on a symbol-by-symbol basis and detects each symbol by finding the constellation point closest to the received sample in terms of Euclidean distance [115, Ch. 3.4]. This can be geometrically interpreted as the use of decision regions in the complex-valued signal space, depicted in Fig. 3.3 for 16QAM.

LPN can be accounted for when finding the *a posteriori* symbol probabilities, in which case their computation does not reduce to minimizing Euclidean distance. Moreover, performing symbol detection and symbol-to-bit mapping to yield the detected data bits is in general suboptimal in terms of minimizing the BER [174]. If minimum BER is the objective, the MAP bit detector should be used. It has been derived or approximated for various channel models [98, 175].

For coded transmission, data detection is more involved. As discussed in Section 2.5, binary FEC codes are commonly utilized in fiber-optic communications in order to satisfy reliability requirements, where the decoder uses as inputs either soft or hard information about the coded bits. The decoder inputs are provided by the demapper and are based on the *a posteriori* probabilities of the transmitted symbols. These probabilities are typically computed under the assumption that all data-bit sequences are equiprobable and that the only remaining impairment is AWGN. In Paper A, we implement MAP bit detection for coded multichannel transmission in the presence of LPN.



---

## Phase-Noise Compensation

---

The presence of LPN<sup>1</sup> necessitates the use of PNC prior to data detection. The problem of PNC has been studied for a long time in the context of fiber-optic communication systems<sup>2</sup> and continues to be an active area of research [60, 176–184]. This is owing to the increased focus on higher-order modulation formats, which allow for an increased spectral efficiency but come with a higher sensitivity to transmission impairments, in particular LPN.

A strategy for designing PNC algorithms is to use estimation theory and appropriate system models. This chapter first introduces the multichannel phase-noise model that Papers A–E are based on, and provides justification for the model using experimental data from SDM transmission through an MCF. A brief explanation of optimal bit detection for transmission in the presence of AWGN and LPN follows, which serves as a preliminary to Paper A. Thereafter, an overview will be given of various blind and pilot-aided algorithms found in the literature for single-channel PNC based on heuristic arguments or designed using theoretical frameworks. Moreover, as Papers A–D are centered on PNC for multichannel systems, different PNC strategies for multichannel transmission in the presence of LPN are reviewed. The end of this section details the effect of pilot-symbol positions on the residual LPN after compensation, which relates to Papers B and E.

---

<sup>1</sup>Nonlinear phase noise can also require the use of PNC techniques [99]. However, this thesis focuses on the compensation of LPN.

<sup>2</sup>PNC is also studied in wireless communications for oscillator phase noise.

## 4.1 Multichannel Phase-Noise Model

The papers included in this thesis are all (directly or indirectly) based on a model that describes LPN in multiple channels. The simplicity of the model facilitates the design of high-performance receiver algorithms that perform joint-channel PNC, but the model is general enough so that the designed algorithms can operate effectively for LPN with arbitrary channel-wise correlation. The model entails transmission of symbol blocks of length  $N_s$  over  $N_{\text{ch}}$  channels, where channel interference, CD, nonlinearities, and carrier-frequency offsets are assumed to be effectively mitigated in DSP, leaving only LPN and AWGN as the remaining signal impairments<sup>3</sup>. With one sample per symbol, the discrete-time and complex baseband signal is expressed in each channel as

$$\mathbf{r}_{i,k} = \mathbf{s}_{i,k} e^{j\boldsymbol{\theta}_{i,k}} + \mathbf{n}_{i,k} \quad (4.1)$$

for channel and time indices  $i = 1, \dots, N_{\text{ch}}$  and  $k = 1, \dots, N_s$ , where  $\mathbf{r}_{i,k}$  is the received sample,  $\mathbf{s}_{i,k}$  is the transmitted symbol,  $\boldsymbol{\theta}_{i,k}$  is the LPN, and  $\mathbf{n}_{i,k}$  is complex AWGN. The LPN across all channels at time  $k$ ,  $\boldsymbol{\theta}_k$ , is approximated as a multidimensional Gaussian random walk as

$$\boldsymbol{\theta}_k = \boldsymbol{\theta}_{k-1} + \Delta\boldsymbol{\theta}_k, \quad (4.2)$$

where  $\boldsymbol{\theta}_1$  is uniformly distributed in  $[0, 2\pi)^{N_{\text{ch}}}$ , and the random-walk innovation  $\Delta\boldsymbol{\theta}_k$  is a multivariate Gaussian random variable with zero mean and covariance matrix  $\mathbf{Q}$ , which describes the channel-wise correlation of the LPN.

The choice of this model is justified by a case study involving experimental SDM transmission<sup>4</sup> of PDM-64QAM through three cores of a weakly-coupled, homogeneous, single-mode MCF. Fig. 4.1 depicts a histogram of the received complex signal in one core and polarization at different points in the DSP chain<sup>5</sup>. When the signal has undergone the first two steps, it can be approximated by (4.1). However, as Fig. 4.1 shows, the signal has residual I/Q imbalance originating from the transmitter, which is not accounted for in the model. Such I/Q imbalances, although not always present, can be compensated through an additional orthonormalization step before data detection. Moreover, Fig. 4.2 shows the estimated LPN in all polarizations and cores, which is approximated by (4.2).

## 4.2 Optimal Detection in the Presence of Phase Noise

MAP bit detection is an optimal strategy in the sense that it minimizes the resulting BER [185, Ch. 1.4]. It performs detection on a bit-by-bit basis by computing

$$\hat{b}_l = \underset{b_l \in \{0,1\}}{\operatorname{argmax}} P_{b_l|\mathbf{r}}(b_l|\mathbf{r}), \quad (4.3)$$

<sup>3</sup>See Paper A for further details on assumptions made in the model.

<sup>4</sup>The data from this experiment is used in Paper C.

<sup>5</sup>See Paper C for more details on the DSP steps.

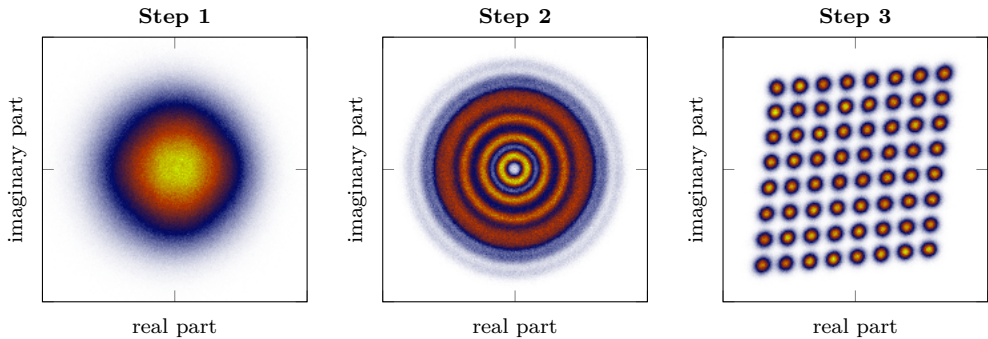


**Figure 4.1:** The received signal at different points in the DSP chain. Step 1: After CD compensation and orthonormalization. Step 2: After timing recovery, adaptive equalization, matched filtering, and frequency-offset compensation. Step 3: After PNC.

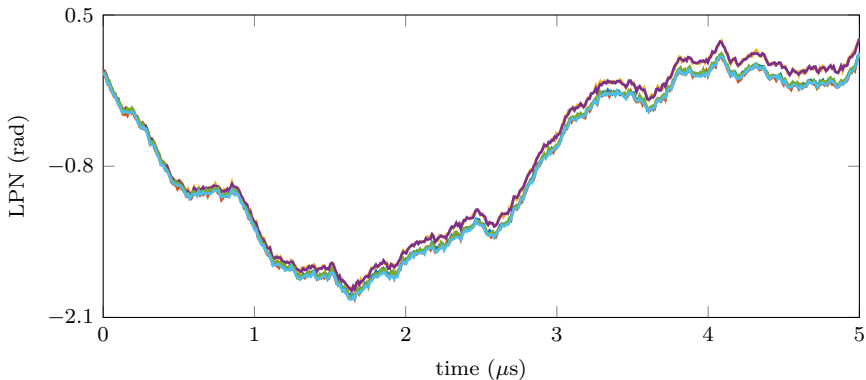


**Figure 4.2:** The estimated LPN in all cores and polarizations over 5  $\mu\text{s}$ , taken from experimental data used in paper C and normalized to start at zero.

where  $\mathbf{b}_l$  is the information bit,  $\mathbf{r}$  comprises all received samples, and  $P_{\mathbf{b}_l|\mathbf{r}}(b_l|\mathbf{r})$  is the *a posteriori* PMF of  $\mathbf{b}_l$  at  $b_l$  given  $\mathbf{r} = \mathbf{r}$ . For trivial scenarios such as uncoded transmission over the AWGN channel, the PMF in (4.3) is mathematically tractable. However, for more complicated models, obtaining  $P_{\mathbf{b}_l|\mathbf{r}}(b_l|\mathbf{r})$  is nontrivial.

Consider a block of  $K$  information bits,  $\mathbf{b} = [\mathbf{b}_1, \dots, \mathbf{b}_K]$  that is mapped to  $N_s N_{\text{ch}}$  symbols through a deterministic function that represents the FEC code and modulation format. The symbols are transmitted over  $N_{\text{ch}}$  channels and the received signal is described by (4.1). Assume that all transmitted symbols, LPN samples, and received samples are encapsulated by  $\mathbf{s}$ ,  $\boldsymbol{\theta}$ , and  $\mathbf{r}$ , respectively. For this model,  $P_{\mathbf{b}_l|\mathbf{r}}(b_l|\mathbf{r})$  is hard to compute due to the presence of an FEC code and LPN, but it can be obtained by marginalizing the joint distribution of all the system parameters,  $p_{\mathbf{b}, \mathbf{s}, \boldsymbol{\theta}|\mathbf{r}}(\mathbf{b}, \mathbf{s}, \boldsymbol{\theta}|\mathbf{r})$ , over all  $\mathbf{s}$ ,  $\boldsymbol{\theta}$ , and  $\mathbf{b}$  except for  $b_l$  [175]. Carrying out this marginalization exactly yields a MAP

bit detection algorithm that jointly performs PNC and decoding. It is interesting to note that it treats the phase noise as a nuisance parameter [186, Ch. 10.7], i.e.,  $\theta$  is simply integrated out. As a consequence, explicit phase-noise estimates are not needed.

Solving the marginalization in closed form is hard in general, and numerical evaluation is impractical due to the presence of integrals. However, several Bayesian inference techniques and frameworks can be used to carry out the marginalization approximately but efficiently. Examples include the expectation–maximization [187] algorithm, variational Bayesian (VB) inference [188], factor graphs (FGs) and the sum–product algorithm (SPA) [189], and various sequential Monte Carlo methods [190]. Two of these examples, namely the FG/SPA and VB frameworks, are used to develop the proposed algorithms in Paper A. The algorithms do not obtain explicit phase-noise estimates, but instead, the *a posteriori* PDFs are estimated through extended Kalman smoothing [191, Ch. 8.2] and used when computing the decoder inputs.

## 4.3 Single-Channel Processing

### 4.3.1 Blind Algorithms

As previously mentioned, pilot symbols do not carry any data and thus reduce the overall spectral efficiency of the system. To avoid the reduction in spectral efficiency, most PNC algorithms in fiber-optic communications have traditionally been blind. Moreover, to simplify implementations in hardware, algorithms are often designed to operate in a feedforward manner, i.e., without containing any feedback loops [124].

Although blind algorithms have no *a priori* knowledge of the transmitted symbols, the structure of some modulation formats can be exploited to allow estimating the LPN. As an example, *MPSK* comprises  $M$  equispaced constellation points on a circle in the complex plane. When observations corresponding to this modulation are raised to the  $M$ th power, the modulation is removed and the LPN can be estimated in a range of length  $2\pi/M$ . The phase-noise estimates are processed and then used to derotate the signal, which mitigates the LPN. To illustrate the concept, Fig. 4.3 shows the general steps used by these techniques for QPSK. The Viterbi–Viterbi algorithm [192] and similar feedforward methods [125, 179] are based on this concept and work effectively for QPSK. However, for higher-order QAM, these methods work suboptimally as the constellation points generally do not have equispaced phases. Among the most widely-used blind algorithms in fiber-optic communications for QAM is the blind phase search (BPS) [124], a feedforward algorithm that yields good performance in terms of laser linewidth tolerance but has a high computational complexity for higher-order formats. Several BPS variants have been proposed that reduce the required computational complexity while maintaining the performance of the original method [193–196]. Furthermore, in the case of higher-order QAM, PNC based on QPSK partitioning [197], decision-directed least-mean square filtering [198], or principal component analysis [183, 199] has been proposed.

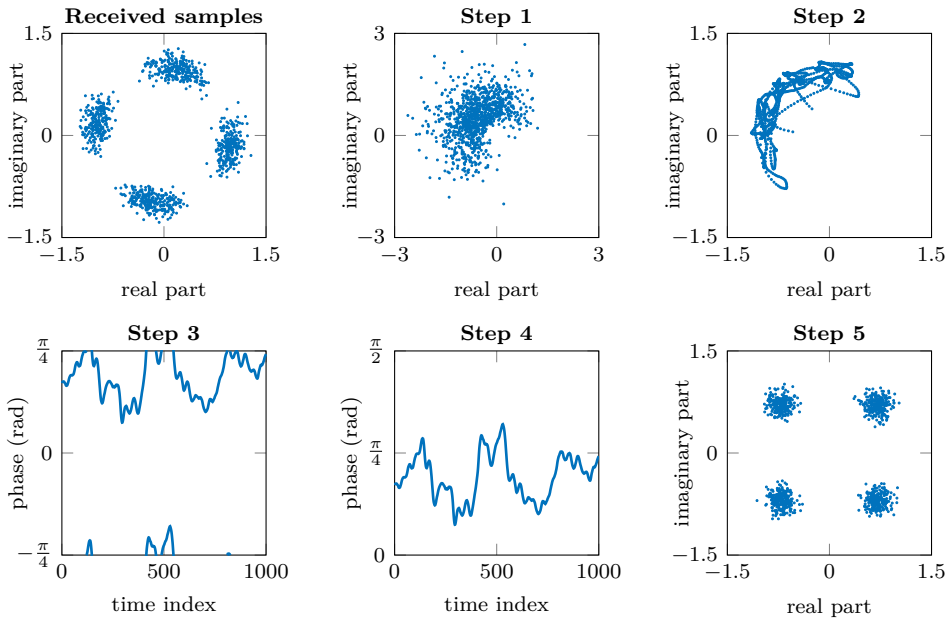


**Figure 4.3:** Illustration of PNC using the  $M$ th-power method for QPSK. Step 1: Raise the received complex samples to the 4th power to remove the phase modulation. Step 2: Filter the 4th-power samples to mitigate distortions from the AWGN. Step 3: Take the angle of the filtered samples and divide by four, which yields wrapped phase-noise estimates in a range of length  $\pi/2$ . Step 4: Unwrap the estimates. Step 5: Derotate the received samples to obtain phase-noise compensated samples.

An inherent problem with blind algorithms is ambiguity in the estimated LPN. Due to the rotational symmetry that is associated with most modulation formats, the LPN can only be estimated unambiguously in a limited range. As a consequence, the phase-noise estimates need to be unwrapped, which is done recursively and thus adds a feedback mechanism to the system. This can lead to cycle slips for low SNRs or sufficient levels of LPN, which in turn causes bursts of errors [125]. Multiple solutions to this have been proposed, e.g., differential encoding [200], which increases the BER in the absence of cycle slips [125], and cycle-slip mitigation using hybrid-modulation techniques [201] or pilots [202].

### 4.3.2 Pilot-Aided Algorithms

An alternative to blind estimation is to use pilot-aided algorithms that are independent of the modulation and yield unambiguous estimates of the LPN. Pilot-aided algorithms have been researched extensively, particularly in the context of wireless communications.

However, they have also gained significant traction in the optical literature recently<sup>6</sup> due to their high performance, which becomes beneficial for transmission of higher-order QAM.

Many examples can be found where pilot-aided algorithms are derived using probabilistic inference frameworks that approximate optimal detection in the presence of phase noise, exploiting the statistical structure of the system model. In [99], an algorithm that compensates for LPN and nonlinear phase noise for WDM transmission with ideal distributed Raman amplification is proposed using probabilistic arguments. Moreover, considering coded transmission in the presence of phase noise, [98, 127] use the FG and SPA framework [189] to derive algorithms that perform iterative phase-noise estimation and decoding. A similar scenario is considered in [126] where the VB framework [188] is used to derive an iterative algorithm. In [209], the algorithm proposed in [98, Sec. IV-B] is extended to perform joint-polarization PNC for PDM transmission. A method based on Kalman filtering [210] and the expectation–maximization [187] algorithm is proposed in [211] and experimentally validated. In [208], PNC is implemented through phase interpolation between the pilots. Finally, a literature review of various symbol detectors for transmission in the presence of phase noise is given in [212].

## 4.4 Joint-Channel Processing

Multichannel transmission plays an important role in fiber-optic communications and has existed for decades in the form of WDM systems, where multiple carriers of different wavelengths are transmitted simultaneously over the same spatial channel. Furthermore, thanks to the coherent receiver and DSP, PDM transmission can be realized where the two polarizations of each carrier are used to transmit independent data. More recently, SDM transmission has gained significant research interest, in which multiple spatial channels are transmitted simultaneously at the same wavelength. Multichannel transmission is also an integral part of wireless MIMO communication systems.

Certain transmission impairments, in particular LPN, are highly correlated across the multiplexed channels in various multichannel transmission scenarios, e.g., SDM systems using specific types of fibers where all spatial channels share the light source and LO lasers [56, 72], WDM systems using frequency combs to act as a light source and LO for all wavelength channels [213], and electrically generated subcarrier systems [214]. The channel-wise correlation in the LPN can be exploited to reduce computational complexity in DSP, e.g., through specialized transmission techniques such as self-homodyne detection [45, 59], where a pilot tone, i.e., an unmodulated carrier, is transmitted in one channel and used as an LO at the receiver, thereby canceling the LPN that originates on the transmitter side. Moreover, DSP-based methods such as master–slave processing [56] can be used, where phase-noise estimation is performed on a single selected channel and the resulting estimates are used to compensate for the LPN in all channels. These methods

---

<sup>6</sup>Pilot rates used in recent literature have typically been 3% or less [86, 203–208].

rely on the LPN being identical across all channels, which is typically not the case in reality due to system characteristics/imperfections and environmental factors [215]; hence, their performance may suffer.

Alternatively to reducing complexity, performance can be improved in terms of linewidth tolerance by exploiting the channel-wise LPN correlation through joint-channel processing, which entails estimating the LPN collectively across all the channels. The improved tolerance can be used to increase power/spectral efficiency, relax laser requirements, or extend transmission reach, at the cost of added computational complexity. The rest of this section discusses joint-channel PNC for perfect and partial phase-noise correlation.

#### 4.4.1 Perfect Phase-Noise Correlation

Ideally, the LPN is fully correlated across the channels, in which case joint-channel processing yields the biggest benefits. To quantify the gains, consider the following example pertaining to a specific case of (4.1), i.e., transmission over  $N_{\text{ch}}$  parallel channels, each containing  $N_s$  independent symbols, assuming identical LPN in all channels. The discrete-time observation at time  $k$  is

$$\mathbf{r}_k = \underline{\mathbf{s}}_k e^{j\boldsymbol{\theta}_k} + \mathbf{n}_k, \quad (4.4)$$

for  $k = 1, \dots, N_s$ , where  $\underline{\mathbf{s}}_k = [\mathbf{s}_{1,k}, \dots, \mathbf{s}_{N_{\text{ch}},k}]^T$  denotes a vector of independent symbols at time  $k$ . Each data symbol is modeled as a random variable, drawn uniformly from a set of constellation points, whereas pilot symbols take on a complex value, known to both the transmitter and the receiver. The average symbol energy of the constellation is  $E_s$ . Furthermore,  $\mathbf{n}_k$  denotes a vector containing samples of complex AWGN with variance  $N_0$  and  $\boldsymbol{\theta}_k$  is LPN, modeled as a random walk, i.e.,  $\boldsymbol{\theta}_k = \boldsymbol{\theta}_{k-1} + \Delta\boldsymbol{\theta}_k$ , where  $\Delta\boldsymbol{\theta}_k$  is a Gaussian random variable with variance  $\sigma^2 = 2\pi\Delta\nu T_s$ , for a combined laser linewidth  $\Delta\nu$  and symbol rate  $1/T_s$ .

This ideal model allows trivially extending single-channel PNC algorithms such that they essentially perform estimate averaging across the channels. As an example, the BPS [124] can be extended as follows. Starting with an initial estimate  $\hat{\boldsymbol{\theta}}_0$  (e.g., obtained from a pilot sequence), the algorithm sequentially determines estimates of the LPN. At time  $k$ , the observation vector  $\mathbf{r}_k$  is rotated by  $L$  test phases,  $\phi_l = \hat{\boldsymbol{\theta}}_{k-1} + \pi l/(2L)$ ,  $l = -L/2 + 1, \dots, L/2$ . Denoting the corresponding hard decision after rotation by  $\hat{\mathbf{x}}_{k,l}$ , the most probable test phase is then found by solving

$$\hat{l}_k = \underset{l}{\operatorname{argmin}} \sum_{n=k-M/2}^{k+M/2} \|\hat{\mathbf{x}}_{n,l} - \mathbf{r}_n \exp(j\phi_l)\|^2, \quad (4.5)$$

where  $M$  determines an observation window in the time domain<sup>7</sup>. Finally, the estimate

<sup>7</sup>The quantities inside the summation in (4.5) are zero padded such that the observation window is valid for all  $k = 1, \dots, N_s$ .

of the total phase at time  $k$  is given by  $\hat{\theta}_k = \hat{\theta}_{k-1} + \pi \hat{l}_k / (2L)$ , after which the algorithm moves on to time  $k+1$ . The benefit of using multiple channels is the possibility to reduce  $M$  by averaging in the channel domain, rather than in the time domain, thus enabling faster tracking [124].

### 4.4.2 Partial Phase-Noise Correlation

As already mentioned, no system gives rise to perfectly correlated LPN across all channels. Instead, the total phase noise will typically contain a dominant component corresponding to the LPN, in addition to channel-specific phase drifts. As a result, more sophisticated system models and algorithms are needed to properly exploit the partial phase-noise correlation. Joint-channel PNC has been studied for more realistic models in the context of wireless communications [216–218], for fiber-optic WDM transmission using frequency combs [203], and for a general fiber-optic multichannel system in Papers A and B. Moreover, Papers C and D use the same model with an application to SDM transmission over a weakly-coupled MCF. Using one of the algorithms from Paper A, an extensive study on the performance gains through joint-channel PNC is done based on simulations and experiments.

### 4.4.3 Pilot-Symbol Positions

In general, the placements of pilot symbols can heavily influence the performance of pilot-aided estimation algorithms [219–223]. The top plots in Fig. 4.4 demonstrate this for PNC, where one realization of the true and estimated LPN<sup>8</sup> are shown for high SNR and two pilot-symbol distributions with 1% overall pilot rate. Paper B studies this problem for PNC in a multichannel setting, where finding effective pilot distributions over channels and time slots is formulated as a discrete optimization problem. Moreover, the bottom plots in Fig. 4.4 show the ensemble average of the squared residual phase noise, i.e., estimation error, which depends on the pilot-symbol positions. Paper E studies transmitter-side DSP for transmission in the presence of LPN-estimation errors, which leaves behind residual phase noise.

---

<sup>8</sup>The phase-noise estimates are obtained using the proposed algorithm in [98, Sec. IV-B] without decoder feedback.

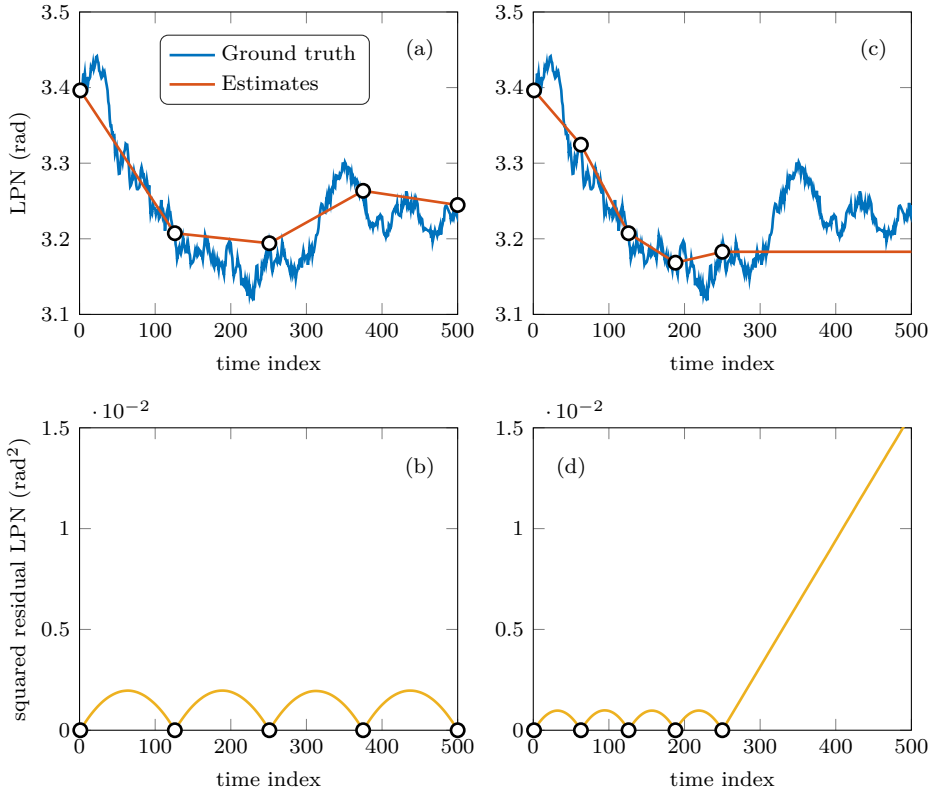


**Figure 4.4:** (a) One realization of the true and estimated LPN, and (b) the ensemble average of the squared estimate error, when the pilots are spaced evenly throughout the symbol block. (c) and (d) show analogous results when the pilots are spaced evenly throughout the first half of the symbol block. The circles correspond to the pilot locations.



This chapter summarizes the contributions of each appended publication and lays out possible directions for future work based on the topics in this thesis.

## 5.1 Paper A

### **“Iterative detection and phase-noise compensation for coded multichannel optical transmission”**

In this paper, motivated by the fact that various multichannel fiber-optic systems have highly correlated LPN across the channels, we address the problem of optimal bit detection for multichannel coded optical transmission in the presence of arbitrarily-correlated LPN. We propose two pilot-aided approximations to the optimal bit detector using different frameworks that can be utilized to simplify Bayesian-inference problems. Moreover, the LPN is modeled as a multidimensional Gaussian random walk, and hence, we effectively estimate it jointly for all channels using an extended Kalman smoother. We further show that the system-model linearization imposed by the extended Kalman smoother does not degrade the performance for practical laser linewidths and symbol rates. Finally, the proposed algorithms are compared to each other and to the BPS algorithm in terms of phase-noise tolerance. Simulation results show that the proposed algorithms perform similarly to each other but significantly outperform the BPS algorithm.

*Contributions:* AFA developed the algorithms, obtained the results, and wrote the paper. EA and HW contributed to the derivations and planning the simulations. All

authors reviewed and revised the paper.

*Context:* Sections 2.5, 3.2.5, 4.1, 4.2, and 4.4.2.

## 5.2 Paper B

### “Pilot distributions for joint-channel carrier-phase estimation in multichannel optical communications”

In this paper, we study the problem of efficiently placing pilot symbols over channels and time slots for PNC in multichannel transmission, which is formulated as a discrete optimization problem. Using one of the pilot-aided algorithms from Paper A and considering parametrized pilot distributions, the optimization involves finding pilot-distribution parameters that minimize the MSE of the phase-noise estimates. The optimized distributions are used as benchmarks, and several heuristic constructions of structured pilot distributions are proposed and compared to the benchmarks for different system parameters, such as the LPN correlation between channels. Simulation results show that having the same uniform pilot spreading in all channels is in general suboptimal as it does not properly exploit the channel-wise LPN correlation. It is further shown that by instead using a pilot distribution that performs as well as the optimization benchmark, significant gains in AIR can be achieved for higher-order QAM.

*Contributions:* AFA formulated the problem, performed the simulations, and wrote the paper. EA helped with the problem formulation. All authors reviewed and revised the paper.

*Context:* Sections 4.1, 4.4.2, and 4.4.3.

## 5.3 Paper C

### “Pilot-aided joint-channel carrier-phase estimation in space-division multiplexed multicore fiber transmission”

In this paper, we investigate the benefits of joint-channel PNC for uncoded SDM transmission through an uncoupled-core, homogeneous, single-mode MCF, where the light source and LO lasers are shared for all cores. We particularize the multichannel phase-noise model from Paper A such that it describes a common LPN in addition to core- and polarization-specific phase drifts. Thereafter, one of the proposed algorithms from Paper A is used to implement two PNC strategies, namely per-channel and joint-channel processing. The strategies are compared in terms of phase-noise tolerance using simulations and experimental data, and the performance improvements through joint-channel PNC are translated to gains in power or spectral efficiency, relaxed hardware requirements, and increased transmission reach. Furthermore, strong agreements are observed between experimental and simulation results.

*Contributions:* AFA formulated the problem, performed the simulations, processed the experimental data, and wrote the paper. EA, MK, and HW assisted with the problem formulation. BP, RSL, and GR provided the experimental data. In addition, RSL assisted with the experimental-data processing. All authors reviewed and revised the paper.

*Context:* Sections 2.3.2, 3.2, 4.1, and 4.4.

## 5.4 Paper D

### “On the performance of joint-core carrier-phase estimation in the presence of intercore skew”

In this paper, we study the effects of intercore skew on the performance of joint-core PNC in uncoded SDM transmission using Monte Carlo simulations. In order to do this, we modify the model considered in Paper C to account for skew. We show that the skew leads to intercore phase differences that cannot be described as Gaussian random walks. Furthermore, we use one of the algorithms from Paper A and propose a simple extension such that it performs effectively in the presence of skew. Thereafter, we show that joint-core PNC always performs equally to or better than per-core PNC. We further show that skew heavily impacts the performance of joint-core PNC. In general, the effectiveness of joint-core PNC depends on the relative quality between the light-source and LO lasers, which is quantified by the ratio of the light-source laser linewidth to the LO laser linewidth. In particular, we show that at high SNRs, the relative performance between joint-core and per-core PNC is invariant to the combined laser linewidth. Assuming that the channels are realigned in DSP in the receiver, we find that joint-core PNC is beneficial if the LO linewidth is smaller than the light-source linewidth.

*Contributions:* AFA formulated the problem, performed the simulations, and wrote the paper. EA assisted with the problem analysis. All authors reviewed and revised the paper.

*Context:* Sections 2.6.7, 4.1, and 4.4.2.

## 5.5 Paper E

### “Optimization of transmitter-side signal rotations in the presence of laser phase noise”

In this paper, we investigate rotations of uncoded multidimensional signals transmitted over multiple complex channels in the presence of LPN that is uncorrelated across the channels. We modify the system model from Paper A to further consider the use of imperfect PNC, leaving residual phase noise that is assumed to be Gaussian distributed. Using the model, we numerically optimize the rotations of four-dimensional signals using Monte Carlo simulations for two receiver types. The first type performs near-optimal

joint-channel data detection, whereas the second type performs a derotation of the received multidimensional signal followed by per-channel data detection, which significantly reduces the required computational complexity at the cost of performance. We show that for both receiver types, it is beneficial to apply multidimensional rotations for moderate amounts of LPN. In particular, rotations based on Hadamard matrices yield the same performance as that of the numerically-optimized rotations for moderate LPN. We further study the effects of combining transmitter-side rotations and receiver-side derotations as the dimensionality of Hadamard-rotated signals grows large. We show that this combination results in the residual phase noise manifesting as signal attenuation and additive noise in each complex channel. This effect is found to give an increase in AIRs of up to 0.25 bits per complex symbol for transmission of higher-order QAM.

*Contributions:* AFA and EA formulated the problem. AFA did the analysis, performed the simulations, and wrote the paper. All authors reviewed and revised the paper.

*Context:* Section 3.1, 4.1, and 4.4.3.

## 5.6 Future Work

This thesis has not been concerned with complexity aspects of the proposed schemes, but rather it has focused on potential performance improvements that can be achieved through joint-channel processing for multichannel transmission in the presence of LPN. A crucial next step is to take practical implementation criteria into account, such as the ability to parallelize the computations and the overall power dissipation of the required hardware. This would clarify whether the proposed methods in this thesis can be implemented or if they require modification.

In the experimental data used in Paper C, the core-specific phase drifts come mainly from residual frequency offsets due to the specific setup that was used. The random-walk assumption in the phase-noise model used in Paper C is inaccurate in this case, but the model could be extended to include biased random walks that account for the linear drifts caused by frequency offsets. Using this extended model, the algorithms proposed in Paper A could also be extended to account for these random-walk biases, which would allow for a more effective PNC in the presence of residual frequency offsets. Moreover, I/Q imbalance from the transmitter side was an unforeseen issue when using the algorithm from Paper A to perform PNC and data detection for the experimental data. The algorithm is designed based on the assumption that PNC is the last DSP step prior to data detection. Hence, it had to be slightly modified such that orthonormalization was performed before symbol detection. It is not clear if this modification caused performance degradations to the algorithm. Including transmitted-based I/Q imbalance in the phase-noise model and developing an algorithm that properly takes this impairment into account would potentially clarify this doubt.

The optimization in Paper B is based on the model introduced in Paper A, and hence it does not take into account impairments that may impact the compensation of LPN,

such as nonlinearities, residual frequency offsets, and I/Q imbalance. Including these phenomena in the system model would be an interesting future direction to determine whether the optimal pilot distributions change. Moreover, as pilot-aided algorithms can in general be used for most steps in the DSP chain, pilot distributions could be optimized jointly for the entire DSP chain, which could provide valuable insight into how to design pilot-aided systems.

The algorithms proposed in Paper A could be applied to study the benefits of joint PNC for different multichannel systems with correlated LPN, e.g., WDM-based systems using frequency combs as light sources and LOs. Another direction is to investigate joint-channel PNC for different SDM scenarios than the MCF system explored in Paper C, e.g., systems using coupled-core MCFs, MMFs, or bundles of SMFs. The characteristics of these systems are potentially different from the system considered in Paper C, and it would therefore be interesting to study the benefits of joint-channel PNC for those scenarios.

In paper C, two pilot distributions are used, neither of which is found to attain the performance corresponding to the optimized distribution in Paper B. It would be of interest to consider the best-performing structured distribution from Paper B for the analysis in Paper C. In particular, it could lead to a stronger joint-core PNC performance for MCF transmission in the presence of significant skew.

The transmitter-side rotation scheme considered in paper E is confined to the case where residual LPN is the dominant transmission impairment, and hence, mainly applicable to short-to-medium haul transmission of higher-order modulation formats. Accounting for other effects such as nonlinearities, interchannel interference, CD, and I/Q imbalance would be an interesting extension to the paper. Furthermore, the paper presents several open questions, such as the most effective bit labelings for transmission of rotated constellations in the presence of LPN, as well as the rotation performance of shaped constellations.



---

## Bibliography

---

- [1] D. Crowley, P. Urquhart, and P. Heyer, *Communication in History: Stone-Age Symbols to Social Media*, 7th ed. New York, NY, USA: Routledge, 2018.
- [2] CISCO, “Cisco visual networking index: Forecast and trends, 2017–2022,” <https://www.cisco.com/c/en/us/solutions/collateral/service-provider/visual-networking-index-vni/white-paper-c11-741490.pdf>, Tech. Rep., Feb. 2019, accessed: 2019-12-04.
- [3] T. H. Maiman, “Stimulated optical radiation in ruby,” *Nature*, vol. 187, pp. 493–494, Aug. 1960.
- [4] K. C. Kao and G. A. Hockham, “Dielectric-fibre surface waveguides for optical frequencies,” *Proceedings of the Institution of Electrical Engineers*, vol. 113, no. 7, pp. 1151–1158, Jul. 1966.
- [5] F. P. Kapron, D. B. Keck, and R. D. Maurer, “Radiation losses in glass optical waveguides,” *APL Applied Physics Letters*, vol. 17, no. 10, pp. 423–425, Nov. 1970.
- [6] R. J. Mears, L. Reekie, I. M. Jauncey, and D. N. Payne, “Low-noise erbium-doped fibre amplifier operating at  $1.54\mu\text{m}$ ,” *IET Electronic Letters*, vol. 23, no. 19, pp. 1026–1028, Sep. 1987.
- [7] E. Desurvire, J. R. Simpson, and P. C. Becker, “High-gain erbium-doped traveling-wave fiber amplifier,” *Optics Letters*, vol. 12, no. 11, pp. 888–890, Nov. 1987.
- [8] W. J. Tomlinson, “Wavelength multiplexing in multimode optical fibers,” *Applied Optics*, vol. 16, no. 8, pp. 2180–2194, Aug. 1977.
- [9] R. A. Linke and A. H. Gnauck, “High-capacity coherent lightwave systems,” *IEEE/OSA Journal of Lightwave Technology*, vol. 6, no. 11, pp. 1750–1769, Nov. 1988.

- [10] M. G. Taylor, “Coherent detection method using DSP for demodulation of signal and subsequent equalization of propagation impairments,” *IEEE Photonics Technology Letters*, vol. 16, no. 2, pp. 674–676, Feb. 2004.
- [11] H. Sun, K.-T. Wu, and K. Roberts, “Real-time measurements of a 40 Gb/s coherent system,” *Optics Express*, vol. 16, no. 2, pp. 873–879, Jan. 2008.
- [12] E. Agrell, M. Karlsson, A. R. Chraplyvy, D. J. Richardson, P. M. Krummrich, P. Winzer, K. Roberts, J. K. Fischer, S. J. Savory, B. J. Eggleton, M. Secondini, F. R. Kschischang, A. Lord, J. Prat, I. Tomkos, J. E. Bowers, S. Srinivasan, M. Brandt-Pearce, and N. Gisin, “Roadmap of optical communications,” *Journal of Optics*, vol. 18, no. 6, pp. 1–40, May 2016.
- [13] C. E. Shannon, “A mathematical theory of communication,” *The Bell System Technical Journal*, vol. 27, no. 3, pp. 379–423, Jul. 1948.
- [14] J. M. Kahn and D. A. B. Miller, “Communications expands its space,” *Nature Photonics*, vol. 11, no. 1, pp. 5–8, Jan. 2017.
- [15] R. Kashyap and K. J. Blow, “Observation of catastrophic self-propelled self-focusing in optical fibres,” *IET Electronic Letters*, vol. 24, no. 1, pp. 47–49, Jan. 1988.
- [16] R.-J. Essiambre, G. Kramer, P. J. Winzer, G. J. Foschini, and B. Goebel, “Capacity limits of optical fiber networks,” *IEEE/OSA Journal of Lightwave Technology*, vol. 28, no. 4, pp. 662–701, Feb. 2010.
- [17] X. Zhou, J. Yu, M.-F. Huang, Y. Shao, T. Wang, P. Magill, M. Cvijetic, L. Nelson, M. Birk, G. Zhang, S. Ten, H. B. Matthew, and S. K. Mishra, “32Tb/s (320×114Gb/s) PDM-RZ-8QAM transmission over 580km of SMF-28 ultra-low-loss fiber,” in *Proc. Optical Fiber Communication Conference (OFC)*, Mar. 2009.
- [18] A. Sano, H. Masuda, T. Kobayashi, M. Fujiwara, K. Horikoshi, E. Yoshida, Y. Miyamoto, M. Matsui, M. Mizoguchi, H. Yamazaki, Y. Sakamaki, and H. Ishii, “69.1-Tb/s (432 × 171-Gb/s) C- and extended L-band transmission over 240 km using PDM-16-QAM modulation and digital coherent detection,” in *Proc. Optical Fiber Communication Conference (OFC)*, Mar. 2010, p. PDPB7.
- [19] D. Qian, M.-F. Huang, E. Ip, Y.-K. Huang, Y. Shao, J. Hu, and T. Wang, “101.7-Tb/s (370×294-Gb/s) PDM-128QAM-OFDM transmission over 3×55-km SSMF using pilot-based phase noise mitigation,” in *Proc. Optical Fiber Communication Conference (OFC)*, Mar. 2011, p. PDPB5.
- [20] A. Sano, T. Kobayashi, S. Yamanaka, A. Matsuura, H. Kawakami, Y. Miyamoto, K. Ishihara, and H. Masuda, “102.3-Tb/s (224 × 548-Gb/s) C- and extended L-band all-Raman transmission over 240 km using PDM-64QAM single carrier FDM with

- digital pilot tone,” in *Proc. Optical Fiber Communication Conference (OFC)*, Mar. 2012, p. PDPSC.3.
- [21] J. Renaudier, A. C. Meseguer, A. Ghazisaeidi, P. Tran, R. Rios-Müller, R. Brenot, A. Verdier, F. Blache, K. Mekhazni, B. Duval, H. Debregeas, M. Achouche, A. Boutin, F. Morin, L. Letteron, N. Fontaine, Y. Frignac, and G. Charlet, “First 100-nm continuous-band WDM transmission system with 115Tb/s transport over 100km using novel ultra-wideband semiconductor optical amplifiers,” in *Proc. European Conference on Optical Communication (ECOC)*, Sep. 2017, p. Th.PDP.A.3.
- [22] H. Masuda, E. Yamazaki, A. Sano, T. Yoshimatsu, T. Kobayashi, E. Yoshida, Y. Miyamoto, S. Matsuoka, Y. Takatori, M. Mizoguchi, K. Okada, K. Hagimoto, T. Yamada, and S. Kamei, “13.5-Tb/s (135×111-Gb/s/ch) no-guard-interval coherent OFDM transmission over 6,248 km using SNR maximized second-order DRA in the extended L-band,” in *Proc. Optical Fiber Communication Conference (OFC)*, Mar. 2009, p. PDPB5.
- [23] M. Salsi, H. Mardoyan, P. Tran, C. Koebele, E. Dutisseuil, G. Charlet, and S. Bigo, “155×100Gbit/s coherent PDM-QPSK transmission over 7,200km,” in *Proc. European Conference on Optical Communication (ECOC)*, Sep. 2009.
- [24] J.-X. Cai, Y. Cai, C. R. Davidson, A. Lucero, H. Zhang, D. G. Foursa, O. V. Sinkin, W. W. Patterson, A. Pilipetskii, G. Mohs, and N. S. Bergano, “20 Tbit/s capacity transmission over 6,860 km,” in *Proc. Optical Fiber Communication Conference (OFC)*, Mar. 2011, p. PDPB4.
- [25] M. Mazurczyk, D. G. Foursa, H. G. Batshon, H. Zhang, C. R. Davidson, J.-X. Cai, A. Pilipetskii, G. Mohs, and N. S. Bergano, “30 Tb/s transmission over 6,630 km using 16QAM signals at 6.1 bits/s/Hz spectral efficiency,” in *Proc. European Conference on Optical Communication (ECOC)*, Sep. 2012, p. Th.3.C.2.
- [26] D. G. Foursa, H. G. Batshon, H. Zhang, M. Mazurczyk, J.-X. Cai, O. Sinkin, A. Pilipetskii, G. Mohs, and N. S. Bergano, “44.1 Tb/s transmission over 9,100 km using coded modulation based on 16QAM signals at 4.9 bits/s/Hz spectral efficiency,” in *Proc. European Conference on Optical Communication (ECOC)*, Sep. 2013, p. PD3.E.1.
- [27] A. Ghazisaeidi, L. Schmalen, I. F. de Jauregui, P. Tran, C. Simonneau, P. Brindel, and G. Charlet, “52.9 Tb/s transmission over transoceanic distances using adaptive multi-rate FEC,” in *Proc. European Conference on Optical Communication (ECOC)*, Sep. 2014, p. PD.3.4.
- [28] A. Ghazisaeidi, L. Schmalen, P. Tran, C. Simonneau, E. Awwad, B. Uscumlic, P. Brindel, and G. Charlet, “54.2 Tb/s transoceanic transmission using ultra low

- loss fiber, multi-rate FEC and digital nonlinear mitigation,” in *Proc. European Conference on Optical Communication (ECOC)*, Sep. 2015.
- [29] A. Ghazisaeidi, I. F. de Jauregui Ruiz, R. Rios-Müller, L. Schmalen, P. Tran, P. Brindel, A. C. Meseguer, Q. Hu, F. Buchali, G. Charlet, and J. Renaudier, “Advanced C+L-band transoceanic transmission systems based on probabilistically shaped PDM-64QAM,” *IEEE/OSA Journal of Lightwave Technology*, vol. 35, no. 7, pp. 1291–1299, Apr. 2017.
- [30] J.-X. Cai, H. G. Batshon, M. V. Mazurczyk, O. V. Sinkin, D. Wang, M. Paskov, W. W. Patterson, C. R. Davidson, P. C. Corbett, G. M. Wolter, T. E. Hammon, M. A. Bolshtyansky, D. G. Foursa, and A. N. Pilipetskii, “70.46 Tb/s over 7,600 km and 71.65 Tb/s over 6,970 km transmission in C+L band using coded modulation with hybrid constellation shaping and nonlinearity compensation,” *IEEE/OSA Journal of Lightwave Technology*, vol. 36, no. 1, pp. 114–121, Jan. 2018.
- [31] M. Ionescu, D. Lavery, A. Edwards, E. Sillekens, L. Galdino, D. Semrau, R. I. Killely, W. Pelouch, S. Barnes, and P. Bayvel, “74.38 Tb/s transmission over 6300 km single mode fiber with hybrid EDFA/Raman amplifiers,” in *Proc. Optical Fiber Communication Conference (OFC)*, Mar. 2019, p. Tu3F.3.
- [32] D. J. Richardson, J. M. Fini, and L. E. Nelson, “Space-division multiplexing in optical fibres,” *Nature Photonics*, vol. 7, no. 5, pp. 354–362, Apr. 2013.
- [33] S. Iano, T. Sato, S. Sentsui, T. Kuroha, and Y. Nishimura, “Multicore optical fiber,” in *Proc. Optical Fiber Communication Conference (OFC)*, Mar. 1979, p. WB1.
- [34] G. P. Agrawal, *Fiber-optic communications systems*, 3rd ed. Hoboken, NJ, USA: John Wiley & Sons, Inc., 2002.
- [35] A. K. Majumdar, *Advanced Free Space Optics (FSO)*. New York City, NY, USA: Springer, 2015.
- [36] K. Xu, D. Cheng, and X. Huang, “Multimode communication system used in local area network(LAN),” in *Proc. Symposium on Photonics and Optoelectronics (SOPO)*, Aug. 2009.
- [37] P. J. Winzer, “High-spectral-efficiency optical modulation formats,” *IEEE/OSA Journal of Lightwave Technology*, vol. 30, no. 24, pp. 3824–3835, Dec. 2012.
- [38] A. M. Joshi, S. Datta, and A. Crawford, “Next-gen communications fiber: Multilevel modulation formats push capacities beyond 100 Gbit/s,” *Laser Focus World*, vol. 48, no. 2, pp. 58–63, 2012.
- [39] G. Agrawal, *Nonlinear Fiber Optics*, 4th ed. New York City, NY, USA: Elsevier Science, 2007.

- 
- [40] P. K. A. Wai and C. R. Menyak, "Polarization mode dispersion, decorrelation, and diffusion in optical fibers with randomly varying birefringence," *IEEE/OSA Journal of Lightwave Technology*, vol. 14, no. 2, pp. 148–157, Feb. 1996.
- [41] P. J. Winzer, D. T. Neilson, and A. R. Chraplyvy, "Fiber-optic transmission and networking: the previous 20 and the next 20 years," *Optics Express*, vol. 26, no. 18, pp. 24 190–24 239, Sep. 2018.
- [42] J. Pfeifle, V. Brasch, M. Lauer mann, Y. Yu, D. Wegner, T. Herr, K. Hartinger, P. Schindler, J. Li, D. Hillerkuss, R. Schmogrow, C. Weimann, R. Holzwarth, W. Freude, J. Leuthold, T. J. Kippenberg, and C. Koos, "Coherent terabit communications with microresonator Kerr frequency combs," *Nature Photonics*, vol. 8, no. 5, pp. 375–380, May 2014.
- [43] G. Bosco, V. Curri, A. Carena, P. Poggiolini, and F. Forghieri, "On the performance of Nyquist-WDM terabit superchannels based on PM-BPSK, PM-QPSK, PM-8QAM or PM-16QAM subcarriers," *IEEE/OSA Journal of Lightwave Technology*, vol. 29, no. 1, pp. 53–61, Jan. 2011.
- [44] X. Yi, N. K. Fontaine, R. P. Scott, and S. J. B. Yoo, "Tb/s coherent optical OFDM systems enabled by optical frequency combs," *IEEE/OSA Journal of Lightwave Technology*, vol. 28, no. 14, pp. 2054–2061, Jul. 2010.
- [45] A. Lorences-Riesgo, T. A. Eriksson, A. Fülöp, P. A. Andrekson, and M. Karlsson, "Frequency-comb regeneration for self-homodyne superchannels," *IEEE/OSA Journal of Lightwave Technology*, vol. 34, no. 8, pp. 1800–1806, Apr. 2016.
- [46] M. Mazur, A. Lorences-Riesgo, J. Schröder, P. A. Andrekson, and M. Karlsson, "10 Tb/s PM-64QAM self-homodyne comb-based superchannel transmission with 4% shared pilot tone overhead," *IEEE/OSA Journal of Lightwave Technology*, vol. 36, no. 16, pp. 3176–3184, Aug. 2018.
- [47] —, "High spectral efficiency PM-128QAM comb-based superchannel transmission enabled by a single shared optical pilot tone," *IEEE/OSA Journal of Lightwave Technology*, vol. 36, no. 6, pp. 1318–1325, Mar. 2018.
- [48] K. Zhanette, J. C. Cartledge, and M. O'Sullivan, "Correlation properties of the phase noise between pairs of lines in a quantum-dot optical frequency comb source," in *Proc. Optical Fiber Communication Conference (OFC)*, Mar. 2017, p. Th3I.6.
- [49] G. Vedala, M. Al-Qadi, M. O'Sullivan, J. Cartledge, and R. Hui, "Phase noise characterization of a QD-based diode laser frequency comb," *Optics Express*, vol. 25, no. 14, pp. 15 890–15 904, Jul. 2017.

- [50] L. Lundberg, M. Karlsson, A. Lorences-Riesgo, M. Mazur, V. Torres-Company, J. Schröder, and P. A. Andrekson, “Frequency comb-based WDM transmission systems enabling joint signal processing,” *MDPI Applied Sciences*, vol. 8, no. 5, p. 718, May 2018.
- [51] B. J. Puttnam, G. Rademacher, R. S. Luís, T. A. Eriksson, W. Klaus, Y. Awaji, N. Wada, K. Maeda, S. Takasaka, and R. Sugizaki, “0.715 Pb/s transmission over 2,009.6 km in 19-core cladding pumped EDFA amplified MCF link,” in *Proc. Optical Fiber Communication Conference (OFC)*, Mar. 2019, p. Th4B.1.
- [52] M. D. Feuer, L. E. Nelson, K. Abedin, X. Zhou, T. F. Taunay, J. F. Fini, B. Zhu, R. Isaac, R. Harel, G. Cohen, and D. M. Marom, “ROADM system for space division multiplexing with spatial superchannels,” in *Proc. Optical Fiber Communication Conference (OFC)*, Mar. 2013, p. PDP5B.8.
- [53] Y. Jung, J. R. Hayes, S. U. Alam, and D. J. Richardson, “Multicore fibre fan-in/fan-out device using fibre optic collimators,” in *Proc. European Conference on Optical Communication (ECOC)*, Sep. 2017, p. P1.SC1.17.
- [54] S. G. Leon-Saval, N. K. Fontaine, and R. Amezcua-Correa, “Photonic lantern as mode multiplexer for multimode optical communications,” *Optical Fiber Technology*, vol. 35, pp. 46–55, Feb. 2017.
- [55] N. K. Fontaine, B. Huang, Z. S. Eznavah, H. Chen, J. Cang, B. Ercan, A. Velaquez-Benitez, S. H. Chang, R. Ryf, A. Schulzgen, J. C. A. Zaharias, P. Sillard, C. Gonnet, J. E. A. Lopez, and R. Amezcua-Correa, “Multi-mode optical fiber amplifier supporting over 10 spatial modes,” in *Proc. Optical Fiber Communication Conference (OFC)*, Mar. 2016, p. Th5A.4.
- [56] M. D. Feuer, L. E. Nelson, X. Zhou, S. L. Woodward, R. Isaac, B. Zhu, T. F. Taunay, M. Fishteyn, J. M. Fini, and M. F. Yan, “Joint digital signal processing receivers for spatial superchannels,” *IEEE Photonics Technology Letters*, vol. 24, no. 21, pp. 1957–1960, Nov. 2012.
- [57] R. S. Luís, B. J. Puttnam, G. Rademacher, W. Klaus, E. Agrell, Y. Awaji, and N. Wada, “On the spectral efficiency limits of crosstalk-limited homogeneous single-mode multi-core fiber systems,” in *Proc. Advanced Photonics*, Jul. 2017, p. NeTu2B.2.
- [58] R. S. Luís, B. J. Puttnam, J.-M. Delgado Mendinueta, Y. Awaji, and N. Wada, “Impact of spatial channel skew on the performance of spatial-division multiplexed self-homodyne transmission systems,” in *Proc. International Conference on Photonics in Switching (PS)*, Sep. 2015, pp. 37–39.

- 
- [59] B. J. Puttnam, J. Sakaguchi, J.-M. Delgado Mendinueta, W. Klaus, Y. Awaji, N. Wada, A. Kanno, and T. Kawanishi, “Investigating self-homodyne coherent detection in a 19 channel space-division-multiplexed transmission link,” *Optics Express*, vol. 21, no. 2, pp. 1561–1566, Jan. 2013.
- [60] L. Lundberg, B. J. Puttnam, R. S. Luís, G. Rademacher, M. Karlsson, P. A. Andreksson, Y. Awaji, and N. Wada, “Master-slave carrier recovery for M-QAM multicore fiber transmission,” *Optics Express*, vol. 27, no. 16, pp. 22 226–22 236, Aug. 2019.
- [61] B. J. Puttnam, T. A. Eriksson, J.-M. Delgado Mendinueta, R. S. Luís, Y. Awaji, N. Wada, M. Karlsson, and E. Agrell, “Modulation formats for multi-core fiber transmission,” *Optics Express*, vol. 22, no. 26, pp. 32 457–32 469, Dec. 2014.
- [62] B. J. Puttnam, R. S. Luís, W. Klaus, J. Sakaguchi, J.-M. Delgado Mendinueta, Y. Awaji, N. Wada, Y. Tamura, T. Hayashi, M. Hirano, and J. Marciante, “2.15 Pb/s transmission using a 22 core homogeneous single-mode multi-core fiber and wideband optical comb,” in *Proc. European Conference on Optical Communication (ECOC)*, Sep. 2015, p. PDP.3.1.
- [63] A. Turukhin, H. G. Batshon, M. Mazurczyk, Y. Sun, C. R. Davidson, J.-X. Chai, O. V. Sinkin, W. Patterson, G. Wolter, M. A. Bolshtyansky, D. G. Foursa, and A. Pilipetskii, “Demonstration of 0.52 Pb/s potential transmission capacity over 8,830 km using multicore fiber,” in *Proc. European Conference on Optical Communication (ECOC)*, Sep. 2016, p. Tu.1.D.3.
- [64] M. Koshihara, K. Saitoh, and Y. Kokubun, “Heterogeneous multi-core fibers: proposal and design principle,” *IEICE Electronics Express*, vol. 6, no. 2, pp. 98–103, Jan. 2009.
- [65] S. Matsuo, K. Takenaga, Y. Sasaki, Y. Amma, S. Saito, K. Saitoh, T. Matsui, K. Nakajima, T. Mizuno, H. Takara, Y. Miyamoto, and T. Morioka, “High-spatial-multiplicity multicore fibers for future dense space-division-multiplexing systems,” *IEEE/OSA Journal of Lightwave Technology*, vol. 34, no. 6, pp. 1464–1475, Mar. 2016.
- [66] J. Sakaguchi, W. Klaus, Y. Awaji, N. Wada, T. Hayashi, T. Nagashima, T. Nakanishi, T. Taru, T. Takahata, and T. Kobayashi, “228-spatial-channel bi-directional data communication system enabled by 39-core 3-mode fiber,” *IEEE/OSA Journal of Lightwave Technology*, vol. 37, no. 8, pp. 1756–1763, Apr. 2019.
- [67] T. Sakamoto, T. Mori, M. Wada, T. Yamamoto, F. Yamamoto, and K. Nakajima, “Strongly-coupled multi-core fiber and its optical characteristics for MIMO transmission systems,” *Optical Fiber Technology*, vol. 35, pp. 8–18, Feb. 2017.

- [68] J.-I. Sakai, K. Kitayama, M. Ikeda, Y. Kato, and T. Kimura, “Design considerations of broadband dual-mode optical fibers,” *IEEE Transactions on Microwave Theory and Techniques*, vol. 26, no. 9, pp. 658–665, Sep. 1978.
- [69] S. Ö. Arık, K.-P. Ho, and J. M. Kahn, “Optical network scaling: roles of spectral and spatial aggregation,” *Optics Express*, vol. 22, no. 24, pp. 29 868–29 887, Dec. 2014.
- [70] C. Antonelli, O. Golani, M. Shtaif, and A. Mecozzi, “Nonlinear interference noise in space-division multiplexed transmission through optical fibers,” *Optics Express*, vol. 25, no. 12, pp. 13 055–13 078, Jun. 2017.
- [71] R. Ryf, N. K. Fontaine, S. Wittek, K. Choutagunta, M. Mazur, H. Chen, J. Carlos Alvarado-Zacarias, R. Amezcua-Correa, M. Capuzzo, R. Kopf, A. Tate, H. Safar, C. Bolle, D. T. Neilson, E. Burrows, K. Kim, M. Bigot-Astruc, F. Achten, P. Sillard, A. Amezcua-Correa, J. M. Kahn, J. Schröder, and J. Carpenter, “High-spectral-efficiency mode-multiplexed transmission over graded-index multimode fiber,” in *Proc. European Conference on Optical Communication (ECOC)*, Sep. 2018.
- [72] R. G. H. van Uden, C. M. Okonkwo, V. A. J. M. Sleiffer, M. Kuschnerov, H. de Waardt, and A. M. J. Koonen, “Single DPLL joint carrier phase compensation for few-mode fiber transmission,” *IEEE Photonics Technology Letters*, vol. 25, no. 14, pp. 1381–1384, Jul. 2013.
- [73] R. G. H. van Uden, C. M. Okonkwo, H. Chen, H. de Waardt, and A. M. J. Koonen, “28-GBd 32QAM FMF transmission with low complexity phase estimators and single DPLL,” *IEEE Photonics Technology Letters*, vol. 26, no. 8, pp. 765–768, Apr. 2014.
- [74] D. Soma, Y. Wakayama, S. Beppu, S. Sumita, T. Tsuritani, T. Hayashi, T. Nagashima, M. Suzuki, M. Yoshida, K. Kasai, M. Nakazawa, H. Takahashi, K. Igarashi, I. Morita, and M. Suzuki, “10.16-peta-b/s dense SDM/WDM transmission over 6-mode 19-core fiber across the C+L band,” *IEEE/OSA Journal of Lightwave Technology*, vol. 36, no. 6, pp. 1362–1368, Mar. 2018.
- [75] E. Agrell and M. Karlsson, “Power-efficient modulation formats in coherent transmission systems,” *IEEE/OSA Journal of Lightwave Technology*, vol. 27, no. 22, pp. 5115–5126, Nov. 2009.
- [76] T. A. Eriksson, P. Johannisson, M. Sjödin, E. Agrell, P. A. Andrekson, and M. Karlsson, “Frequency and polarization switched QPSK,” in *Proc. European Conference on Optical Communication (ECOC)*, Sep. 2013, p. Th.2.D.4.
- [77] M. Karlsson and E. Agrell, “Generalized pulse-position modulation for optical power-efficient communication,” in *Proc. European Conference on Optical Communication (ECOC)*, Sep. 2011, p. Tu.6.B.6.

- 
- [78] C. Laperle and M. O’Sullivan, “Advances in high-speed DACs, ADCs, and DSP for optical coherent transceivers,” *IEEE/OSA Journal of Lightwave Technology*, vol. 32, no. 4, pp. 629–643, Feb. 2014.
- [79] X. Chen, J. Cho, A. Adamiecki, and P. Winzer, “16384-QAM transmission at 10 GBd over 25-km SSMF using polarization-multiplexed probabilistic constellation shaping,” in *Proc. European Conference on Optical Communication (ECOC)*, Sep. 2019, p. PD.3.3.
- [80] T. A. Eriksson, P. Johannisson, E. Agrell, P. A. Andrekson, and M. Karlsson, “Biorthogonal modulation in 8 dimensions experimentally implemented as 2PPM-PS-QPSK,” in *Proc. Optical Fiber Communication Conference (OFC)*, Mar. 2014, p. W1A.5.
- [81] D. S. Millar, T. Koike-Akino, R. Maher, D. Lavery, M. Paskov, K. Kojima, K. Parsons, B. C. Thomsen, S. J. Savory, and P. Bayvel, “Experimental demonstration of 24-dimensional extended Golay coded modulation with LDPC,” in *Proc. Optical Fiber Communication Conference (OFC)*, Mar. 2014, p. M3A.5.
- [82] B. Chen, C. Okonkwo, H. Hafermann, and A. Alvarado, “Polarization-ring-switching for nonlinearity-tolerant geometrically shaped four-dimensional formats maximizing generalized mutual information,” *IEEE/OSA Journal of Lightwave Technology*, vol. 37, no. 14, pp. 3579–3591, Jul. 2019.
- [83] G. Forney, R. Gallager, G. Lang, F. Longstaff, and S. Qureshi, “Efficient modulation for band-limited channels,” *IEEE Journal on Selected Areas in Communications*, vol. 2, no. 5, pp. 632–647, Sep. 1984.
- [84] F. Buchali, G. Böcherer, W. Idler, L. Schmalen, P. Schulte, and F. Steiner, “Experimental demonstration of capacity increase and rate-adaptation by probabilistically shaped 64-QAM,” in *Proc. European Conference on Optical Communication (ECOC)*, Sep. 2015.
- [85] S. Chandrasekhar, B. Li, J. Cho, X. Chen, E. Burrows, G. Raybon, and P. Winzer, “High-spectral-efficiency transmission of PDM 256-QAM with parallel probabilistic shaping at record rate-reach trade-offs,” in *Proc. European Conference on Optical Communication (ECOC)*, Sep. 2016, p. Th.3.C.1.
- [86] A. Ghazisaeidi, I. F. de Jauregui Ruiz, R. Rios-Muller, L. Schmalen, P. Tran, P. Brindel, A. C. Meseguer, Q. Hu, F. Buchali, G. Charlet, and J. Renaudier, “65Tb/s transoceanic transmission using probabilistically-shaped PDM-64QAM,” in *Proc. European Conference on Optical Communication (ECOC)*, Sep. 2016, p. Th.3.C.4.
- [87] J. Cho, X. Chen, S. Chandrasekhar, G. Raybon, R. Dar, L. Schmalen, E. Burrows, A. Adamiecki, S. Corteselli, Y. Pan, D. Correa, B. McKay, S. Zsigmond, P. J. Winzer,

- and S. Grubb, “Trans-atlantic field trial using high spectral efficiency probabilistically shaped 64-QAM and single-carrier real-time 250-Gb/s 16-QAM,” *IEEE/OSA Journal of Lightwave Technology*, vol. 36, no. 1, pp. 103–113, Jan. 2018.
- [88] S. L. Olsson, J. Cho, S. Chandrasekhar, X. Chen, P. J. Winzer, and S. Makovejs, “Probabilistically shaped PDM 4096-QAM transmission over up to 200 km of fiber using standard intradyne detection,” *Optics Express*, vol. 26, no. 4, pp. 4522–4530, Feb. 2018.
- [89] L. Schmalen, A. J. de Lind van Wijngaarden, and S. ten Brink, “Forward error correction in optical core and optical access networks,” *Bell Labs Technical Journal*, vol. 18, no. 3, pp. 39–66, Dec. 2013.
- [90] R. Gallager, “Low-density parity-check codes,” *IRE Transactions on Information Theory*, vol. 8, no. 1, pp. 21–28, Jan. 1962.
- [91] C. Berrou, A. Glavieux, and P. Thitimajshima, “Near Shannon limit error-correcting coding and decoding: Turbo-codes. 1,” in *Proc. IEEE International Conference on Communications (ICC)*, vol. 2, May 1993, pp. 1064–1070.
- [92] E. Arıkan, “Channel polarization: A method for constructing capacity-achieving codes for symmetric binary-input memoryless channels,” *IEEE Transactions on Information Theory*, vol. 55, no. 7, pp. 3051–3073, Jul. 2009.
- [93] A. Alvarado, T. Fehenberger, B. Chen, and F. M. J. Willems, “Achievable information rates for fiber optics: Applications and computations,” *IEEE/OSA Journal of Lightwave Technology*, vol. 36, no. 2, pp. 424–439, Jan. 2018.
- [94] C. Douillard, M. Jézéquel, C. Berrou, D. Electronique, A. Picart, P. Didier, and A. Glavieux, “Iterative correction of intersymbol interference: Turbo-equalization,” *European Transactions on Telecommunications*, vol. 6, no. 5, pp. 507–511, Sep. 1995.
- [95] S. ten Brink, J. Speidel, and Ran-Hong Yan, “Iterative demapping and decoding for multilevel modulation,” in *Proc. Global Communications Conference (GLOBECOM)*, vol. 1, Nov. 1998, pp. 579–584.
- [96] N. Noels, C. Herzet, A. Dejonghe, V. Lottici, H. Steendam, M. Moeneclaey, M. Luise, and L. Vandendorpe, “Turbo synchronization: an EM algorithm interpretation,” in *Proc. IEEE International Conference on Communications (ICC)*, vol. 4, May 2003, pp. 2933–2937.
- [97] C. Pan, H. Bülow, W. Idler, L. Schmalen, and F. R. Kschischang, “Optical nonlinear phase noise compensation for  $9 \times 32$ -Gbaud PolDM-16 QAM transmission using a code-aided expectation-maximization algorithm,” *IEEE/OSA Journal of Lightwave Technology*, vol. 33, no. 17, pp. 3679–3686, Sep. 2015.

- 
- [98] G. Colavolpe, A. Barbieri, and G. Caire, “Algorithms for iterative decoding in the presence of strong phase noise,” *IEEE Journal on Selected Areas in Communications*, vol. 23, no. 9, pp. 1748–1757, Sep. 2005.
- [99] M. P. Yankov, T. Fehenberger, L. Barletta, and N. Hanik, “Low-complexity tracking of laser and nonlinear phase noise in WDM optical fiber systems,” *IEEE/OSA Journal of Lightwave Technology*, vol. 33, no. 23, pp. 4975–4984, Dec. 2015.
- [100] T. A. Eriksson, T. Fehenberger, P. A. Andrekson, M. Karlsson, N. Hanik, and E. Agrell, “Impact of 4D channel distribution on the achievable rates in coherent optical communication experiments,” *IEEE/OSA Journal of Lightwave Technology*, vol. 34, no. 9, pp. 2256–2266, May 2016.
- [101] T. Miya, Y. Terunuma, T. Hosaka, and T. Miyashita, “Ultimate low-loss single-mode fibre at 1.55  $\mu\text{m}$ ,” *IET Electronic Letters*, vol. 15, no. 4, pp. 106–108, Feb. 1979.
- [102] B. G. Bathula, R. K. Sinha, A. L. Chiu, M. D. Feuer, G. Li, S. L. Woodward, W. Zhang, R. Doverspike, P. Magill, and K. Bergman, “Constraint routing and regenerator site concentration in ROADMs networks,” *IEEE/OSA Journal of Optical Communications and Networking*, vol. 5, no. 11, pp. 1202–1214, Nov. 2013.
- [103] O. Gerstel, M. Jinno, A. Lord, and S. J. B. Yoo, “Elastic optical networking: A new dawn for the optical layer?” *IEEE Communications Magazine*, vol. 50, no. 2, pp. 12–20, Feb. 2012.
- [104] R. H. Stolen and E. P. Ippen, “Raman gain in glass optical waveguides,” *APL Applied Physics Letters*, vol. 22, no. 6, pp. 276–278, Mar. 1973.
- [105] M. Secondini and E. Forestieri, “Scope and limitations of the nonlinear Shannon limit,” *IEEE/OSA Journal of Lightwave Technology*, vol. 35, no. 4, pp. 893–902, Feb. 2017.
- [106] A. Mecozzi and M. Shtaif, “The statistics of polarization-dependent loss in optical communication systems,” *IEEE Photonics Technology Letters*, vol. 14, no. 3, pp. 313–315, Mar. 2002.
- [107] B. Huttner, C. Geiser, and N. Gisin, “Polarization-induced distortions in optical fiber networks with polarization-mode dispersion and polarization-dependent losses,” *IEEE Journal of Selected Topics in Quantum Electronics*, vol. 6, no. 2, pp. 317–329, Mar. 2000.
- [108] T. Duthel, C. R. S. Fludger, J. Geyer, and C. Schulien, “Impact of polarisation dependent loss on coherent POLMUX-NRZ-DQPSK,” in *Proc. Optical Fiber Communication Conference (OFC)*, Feb. 2008, p. OTh4E.3.

- [109] X. Liu, A. R. Chraplyvy, P. J. Winzer, R. W. Tkach, and S. Chandrasekhar, "Phase-conjugated twin waves for communication beyond the Kerr nonlinearity limit," *Nature Photonics*, vol. 7, no. 7, pp. 560–568, May 2013.
- [110] S. L. Jansen, D. van den Borne, P. M. Krummrich, S. Spälter, G.-D. Khoe, and H. de Waardt, "Long-haul DWDM transmission systems employing optical phase conjugation," *IEEE Journal of Selected Topics in Quantum Electronics*, vol. 12, no. 4, pp. 505–520, Jul. 2006.
- [111] R.-J. Essiambre, P. J. Winzer, X. Q. Wang, W. Lee, C. A. White, and E. C. Burrows, "Electronic predistortion and fiber nonlinearity," *IEEE Photonics Technology Letters*, vol. 18, no. 17, pp. 1804–1806, Sep. 2006.
- [112] E. Ip, "Nonlinear compensation using backpropagation for polarization-multiplexed transmission," *IEEE/OSA Journal of Lightwave Technology*, vol. 28, no. 6, pp. 939–951, Mar. 2010.
- [113] F. Derr, "Coherent optical QPSK intradyne system: concept and digital receiver realization," *IEEE/OSA Journal of Lightwave Technology*, vol. 10, no. 9, pp. 1290–1296, Sep. 1992.
- [114] K. Petermann, *Laser Diode Modulation and Noise*. Netherlands: Springer Netherlands, 1988.
- [115] U. Madhow, *Fundamentals of Digital Communication*. New York City, NY, USA: Cambridge University Press, 2008.
- [116] C. H. Henry, "Theory of the linewidth of semiconductor lasers," *IEEE Journal of Selected Topics in Quantum Electronics*, vol. 18, no. 2, pp. 259–264, Feb. 1982.
- [117] W. Shieh and K.-P. Ho, "Equalization-enhanced phase noise for coherent-detection systems using electronic digital signal processing," *Optics Express*, vol. 16, no. 20, pp. 15 718–15 727, Sep. 2008.
- [118] S. Bennetts, G. D. McDonald, K. S. Hardman, J. E. Debs, C. C. N. Kuhn, J. D. Close, and N. P. Robins, "External cavity diode lasers with 5kHz linewidth and 200nm tuning range at 1.55 $\mu$ m and methods for linewidth measurement," *Optics Express*, vol. 22, no. 9, pp. 10 642–10 654, May 2014.
- [119] B. J. Puttnam, R. Luis, J.-M. Delgado-Mendinueta, J. Sakaguchi, W. Klaus, Y. Awaji, N. Wada, A. Kanno, and T. Kawanishi, "High-capacity self-homodyne PDM-WDM-SDM transmission in a 19-core fiber," *Optics Express*, vol. 22, no. 18, pp. 21 185–21 191, Sep. 2014.
- [120] I. Fatadin, S. J. Savory, and D. Ives, "Compensation of quadrature imbalance in an optical QPSK coherent receiver," *IEEE Photonics Technology Letters*, vol. 20, no. 20, pp. 1733–1735, Oct. 2008.

- 
- [121] T.-H. Nguyen, P. Scalart, M. Joindot, M. Gay, L. Bramerie, C. Peucheret, A. Carer, J.-C. Simon, and O. Sentieys, “Joint simple blind IQ imbalance compensation and adaptive equalization for 16-QAM optical communications,” in *Proc. IEEE International Conference on Communications (ICC)*, Jun. 2015, pp. 4913–4918.
- [122] G. M. Saridis, B. J. Puttnam, R. S. Luís, W. Klaus, Y. Awaji, G. Zervas, D. Simeonidou, and N. Wada, “Dynamic skew measurements in 7, 19 and 22-core multi core fibers,” in *Proc. OptoElectronics and Communications Conference (OECC)*, Jul. 2016, pp. MC2–1.
- [123] B. J. Puttnam, G. Rademacher, R. S. Luís, J. Sakaguchi, Y. Awaji, and N. Wada, “Inter-core skew measurements in temperature controlled multi-core fiber,” in *Proc. Optical Fiber Communication Conference (OFC)*, Mar. 2018, p. Tu3B.3.
- [124] T. Pfau, S. Hoffmann, and R. Noé, “Hardware-efficient coherent digital receiver concept with feedforward carrier recovery for  $M$ -QAM constellations,” *IEEE/OSA Journal of Lightwave Technology*, vol. 27, no. 8, pp. 989–999, Apr. 2009.
- [125] E. Ip and J. M. Kahn, “Feedforward carrier recovery for coherent optical communications,” *IEEE/OSA Journal of Lightwave Technology*, vol. 25, no. 9, pp. 2675–2692, Sep. 2007.
- [126] M. Nissilä and S. Pasupathy, “Adaptive iterative detectors for phase-uncertain channels via variational bounding,” *IEEE Transactions on Communications*, vol. 57, no. 3, pp. 716–725, Mar. 2009.
- [127] N. Noels, J. Bhatti, H. Bruneel, and M. Moeneclaey, “Block-processing soft-input soft-output demodulator for coded PSK using DCT-based phase noise estimation,” *IEEE Transactions on Communications*, vol. 62, no. 8, pp. 2939–2950, Aug. 2014.
- [128] S. Beppu, K. Kasai, M. Yoshida, and M. Nakazawa, “2048 QAM (66 Gbit/s) single-carrier coherent optical transmission over 150 km with a potential SE of 15.3 bit/s/Hz,” in *Proc. Optical Fiber Communication Conference (OFC)*, Mar. 2014.
- [129] K. Igarashi, D. Souma, Y. Wakayama, K. Takeshima, Y. Kawaguchi, T. Tsuritani, I. Morita, and M. Suzuki, “114 space-division-multiplexed transmission over 9.8-km weakly-coupled-6-mode uncoupled-19-core fibers,” in *Proc. Optical Fiber Communication Conference (OFC)*, Mar. 2015, p. Th5C.4.
- [130] J. Cho, L. Schmalen, and P. J. Winzer, “Normalized generalized mutual information as a forward error correction threshold for probabilistically shaped QAM,” in *Proc. European Conference on Optical Communication (ECOC)*, Sep. 2017, p. M.2.D.2.
- [131] T. Yoshida, M. Karlsson, and E. Agrell, “Performance metrics for systems with soft-decision FEC and probabilistic shaping,” *IEEE Photonics Technology Letters*, vol. 29, no. 23, pp. 2111–2114, Dec. 2017.

- [132] R. I. Killey, P. M. Watts, V. Mikhailov, M. Glick, and P. Bayvel, “Electronic dispersion compensation by signal predistortion using digital processing and a dual-drive Mach-Zehnder modulator,” *IEEE Photonics Technology Letters*, vol. 17, no. 3, pp. 714–716, Mar. 2005.
- [133] R. Rath, D. Clausen, S. Ohlendorf, S. Pachnicke, and W. Rosenkranz, “Tomlinson–Harashima precoding for dispersion uncompensated PAM-4 transmission with direct-detection,” *IEEE/OSA Journal of Lightwave Technology*, vol. 35, no. 18, pp. 3909–3917, Sep. 2017.
- [134] R.-J. Essiambre and P. J. Winzer, “Fibre nonlinearities in electronically pre-distorted transmission,” in *Proc. European Conference on Optical Communication (ECOC)*, vol. 2, Sep. 2005, p. Tu 3.2.2.
- [135] K. Roberts, Chuandong Li, L. Strawczynski, M. O’Sullivan, and I. Hardcastle, “Electronic precompensation of optical nonlinearity,” *IEEE Photonics Technology Letters*, vol. 18, no. 2, pp. 403–405, Jan. 2006.
- [136] L. B. Y. Du and A. J. Lowery, “Fiber nonlinearity precompensation for long-haul links using direct-detection optical OFDM,” *Optics Express*, vol. 16, no. 9, pp. 6209–6215, Apr. 2008.
- [137] A. J. Lowery, “Fiber nonlinearity pre- and post-compensation for long-haul optical links using OFDM,” *Optics Express*, vol. 15, no. 20, pp. 12 965–12 970, Oct. 2007.
- [138] D. Lavery, D. Ives, G. Liga, A. Alvarado, S. J. Savory, and P. Bayvel, “The benefit of split nonlinearity compensation for single-channel optical fiber communications,” *IEEE Photonics Technology Letters*, vol. 28, no. 17, pp. 1803–1806, Sep. 2016.
- [139] E. Awwad, Y. Jaouën, and G. R.-B. Othman, “Polarization-time coding for PDL mitigation in long-haul polmux OFDM systems,” *Optics Express*, vol. 21, no. 19, pp. 22 773–22 790, Sep. 2013.
- [140] C. Zhu, B. Song, B. Corcoran, L. Zhuang, and A. J. Lowery, “Improved polarization dependent loss tolerance for polarization multiplexed coherent optical systems by polarization pairwise coding,” *Optics Express*, vol. 23, no. 21, pp. 27 434–27 447, Oct. 2015.
- [141] T. Oyama, G. Huang, H. Nakashima, Y. Nomura, T. Takahara, and T. Hoshida, “Low-complexity, low-PAPR polarization-time code for PDL mitigation,” in *Proc. Optical Fiber Communication Conference (OFC)*, Mar. 2019, p. W3H.1.
- [142] E. Awwad, G. R. Othman, and Y. Jaouën, “Space-time coding schemes for MDL-impaired mode-multiplexed fiber transmission systems,” *IEEE/OSA Journal of Lightwave Technology*, vol. 33, no. 24, pp. 5084–5094, Dec. 2015.

- 
- [143] C. Zhu, B. Song, L. Zhuang, B. Corcoran, and A. J. Lowery, "Subband pairwise coding for robust Nyquist-WDM superchannel transmission," *IEEE/OSA Journal of Lightwave Technology*, vol. 34, no. 8, pp. 1746–1753, Apr. 2016.
- [144] K. Shibahara, A. Masuda, H. Kishikawa, S. Kawai, and M. Fukutoku, "Filtering-tolerant transmission by the Walsh-Hadamard transform for super-channel beyond 100 Gb/s," *Optics Express*, vol. 23, no. 10, pp. 13 245–13 254, May 2015.
- [145] W.-R. Peng, T. Tsuritani, and I. Morita, "Modified Walsh-Hadamard transform for PDL mitigation," in *Proc. European Conference on Optical Communication (ECOC)*, Sep. 2013.
- [146] K. Shibahara, T. Mizuno, H. Takara, H. Kawakami, D. Lee, Y. Miyamoto, S. Matsuo, K. Saitoh, and M. Yamada, "Space-time coding-assisted transmission for mitigation of MDL impact on mode-division multiplexed signals," in *Proc. Optical Fiber Communication Conference (OFC)*, Mar. 2016, p. Th4C.4.
- [147] T. Tanimura, S. Oda, T. Tanaka, T. Hoshida, Z. Tao, and J. C. Rasmussen, "A simple digital skew compensator for coherent receiver," in *Proc. European Conference on Optical Communication (ECOC)*, Sep. 2009, p. 7.3.2.
- [148] Y. Wang, E. Serpedin, and P. Ciblat, "An alternative blind feedforward symbol timing estimator using two samples per symbol," *IEEE Transactions on Communications*, vol. 51, no. 9, pp. 1451–1455, Sep. 2003.
- [149] R. Dar and P. J. Winzer, "Nonlinear interference mitigation: Methods and potential gain," *IEEE/OSA Journal of Lightwave Technology*, vol. 35, no. 4, pp. 903–930, Feb. 2017.
- [150] R. S. Luís, B. J. Puttnam, G. Rademacher, Y. Awaji, and N. Wada, "On the use of high-order MIMO for long-distance homogeneous single-mode multicore fiber transmission," in *Proc. Optical Fiber Communication Conference (OFC)*, Sep. 2017, p. Th.2.F.2.
- [151] I. Mayer, "On Löwdin's method of symmetric orthogonalization," *International Journal of Quantum Chemistry*, vol. 90, no. 1, pp. 63–65, Feb. 2002.
- [152] S. J. Savory, "Digital coherent optical receivers: Algorithms and subsystems," *IEEE Journal of Selected Topics in Quantum Electronics*, vol. 16, no. 5, pp. 1164–1179, Sep. 2010.
- [153] S. H. Chang, H. S. Chung, and K. Kim, "Impact of quadrature imbalance in optical coherent QPSK receiver," *IEEE Photonics Technology Letters*, vol. 21, no. 11, pp. 709–711, Jun. 2009.

- [154] C. S. Petrou, A. Vgenis, I. Roudas, and L. Raptis, “Quadrature imbalance compensation for PDM QPSK coherent optical systems,” *IEEE Photonics Technology Letters*, vol. 21, no. 24, pp. 1876–1878, Dec. 2009.
- [155] Y. Qiao, Y. Xu, L. Li, and Y. Ji, “Quadrature imbalance compensation algorithm based on statistical properties of signals in CO-QPSK system,” *IEEE Chinese Optics Letters*, vol. 10, no. 12, pp. 120601-1–4, Dec. 2012.
- [156] Q. Zhang, Y. Yang, C. Guo, X. Zhou, Y. Yao, A. P. T. Lau, and C. Lu, “Modulation-format-transparent IQ imbalance estimation of dual-polarization optical transmitter based on maximum likelihood independent component analysis,” *Optics Express*, vol. 27, no. 13, pp. 18 055–18 068, Jun. 2019.
- [157] R. A. Soriano, F. N. Hauske, N. G. Gonzalez, Z. Zhang, Y. Ye, and I. T. Monroy, “Chromatic dispersion estimation in digital coherent receivers,” *IEEE/OSA Journal of Lightwave Technology*, vol. 29, no. 11, pp. 1627–1637, Jun. 2011.
- [158] S. J. Savory, “Digital filters for coherent optical receivers,” *Optics Express*, vol. 16, no. 2, pp. 804–817, Jan. 2008.
- [159] S. J. Savory, G. Gavioli, R. I. Killey, and P. Bayvel, “Electronic compensation of chromatic dispersion using a digital coherent receiver,” *Optics Express*, vol. 15, no. 5, pp. 2120–2126, Mar. 2007.
- [160] G. Goldfarb and G. Li, “Chromatic dispersion compensation using digital IIR filtering with coherent detection,” *IEEE Photonics Technology Letters*, vol. 19, no. 13, pp. 969–971, Jul. 2007.
- [161] M. Kuschnerov, F. N. Hauske, K. Piyawanno, B. Spinnler, M. S. Alfiad, A. Napoli, and B. Lankl, “DSP for coherent single-carrier receivers,” *IEEE/OSA Journal of Lightwave Technology*, vol. 27, no. 16, pp. 3614–3622, Aug. 2009.
- [162] F. N. Hauske, M. Kuschnerov, B. Spinnler, and B. Lankl, “Optical performance monitoring in digital coherent receivers,” *IEEE/OSA Journal of Lightwave Technology*, vol. 27, no. 16, pp. 3623–3631, Aug. 2009.
- [163] H. Wymeersch and P. Johannisson, “Maximum-likelihood-based blind dispersion estimation for coherent optical communication,” *IEEE/OSA Journal of Lightwave Technology*, vol. 30, no. 18, pp. 2976–2982, Sep. 2012.
- [164] F. Pittalà, F. N. Hauske, Y. Ye, N. G. Gonzalez, and I. T. Monroy, “Fast and robust CD and DGD estimation based on data-aided channel estimation,” in *Proc. International Conference on Transparent Optical Networks (ICTON)*, Jun. 2011.
- [165] C. Do, A. V. Tran, and D. F. Hewitt, “Chromatic dispersion estimation based on complementary golay sequences for 80 Gb/s QPSK single-carrier system with

- 
- frequency domain equalization,” in *Proc. Australasian Telecommunication Networks and Applications Conference (ATNAC)*, Nov. 2011.
- [166] D. N. Godard, “Self-recovering equalization and carrier tracking in two-dimensional data communication systems,” *IEEE Transactions on Communications*, vol. 28, no. 11, pp. 1867–1875, Nov. 1980.
- [167] I. Fatadin, D. Ives, and S. J. Savory, “Blind equalization and carrier phase recovery in a 16-QAM optical coherent system,” *IEEE/OSA Journal of Lightwave Technology*, vol. 27, no. 15, pp. 3042–3049, Aug. 2009.
- [168] M. J. Ready and R. P. Gooch, “Blind equalization based on radius directed adaptation,” in *Proc. International Conference on Acoustics, Speech, and Signal Processing (ICASSP)*, vol. 3, Apr. 1990, pp. 1699–1702.
- [169] P. J. Winzer, A. H. Gnauck, C. R. Doerr, M. Magarini, and L. L. Buhl, “Spectrally efficient long-haul optical networking using 112-Gb/s polarization-multiplexed 16-QAM,” *IEEE/OSA Journal of Lightwave Technology*, vol. 28, no. 4, pp. 547–556, Feb. 2010.
- [170] A. Leven, N. Kaneda, U.-V. Koc, and Y.-K. Chen, “Frequency estimation in intradyne reception,” *IEEE Photonics Technology Letters*, vol. 19, no. 6, pp. 366–368, Mar. 2007.
- [171] S. Hoffmann, S. Bhandare, T. Pfau, O. Adamczyk, C. Wördehoff, R. Peveling, M. Pormann, and R. Noé, “Frequency and phase estimation for coherent QPSK transmission with unlocked DFB lasers,” *IEEE Photonics Technology Letters*, vol. 20, no. 18, pp. 1569–1571, Sep. 2008.
- [172] M. Morelli and U. Mengali, “Feedforward frequency estimation for PSK: A tutorial review,” *European Transactions on Telecommunications*, vol. 9, no. 2, pp. 103–116, Mar. 1998.
- [173] M. Selmi, Y. Jaouën, and P. Ciblat, “Accurate digital frequency offset estimator for coherent PolMux QAM transmission systems,” in *Proc. European Conference on Optical Communication (ECOC)*, Sep. 2009, p. P3.08.
- [174] M. K. Simon and R. Annavajjala, “On the optimality of bit detection of certain digital modulations,” *IEEE Transactions on Communications*, vol. 53, no. 2, pp. 299–307, Feb. 2005.
- [175] C. Herzet, N. Noels, V. Lottici, H. Wymeersch, M. Luise, M. Moeneclaey, and L. Vandendorpe, “Code-aided turbo synchronization,” *Proceedings of the IEEE*, vol. 95, no. 6, pp. 1255–1271, Jun. 2007.

- [176] D. A. A. Mello, F. A. Barbosa, and J. D. Reis, “Interplay of probabilistic shaping and the blind phase search algorithm,” *IEEE/OSA Journal of Lightwave Technology*, vol. 36, no. 22, pp. 5096–5105, Nov. 2018.
- [177] F. Liu, Y. Lin, Y. Yu, and L. P. Barry, “Parallelized Kalman filters for mitigation of the excess phase noise of fast tunable lasers in coherent optical communication systems,” *IEEE Photonics Journal*, vol. 10, no. 1, p. 7200511, Feb. 2018.
- [178] F. A. Barbosa and D. A. A. Mello, “Shaping factor detuning for optimized phase recovery in probabilistically-shaped systems,” in *Proc. Optical Fiber Communication Conference (OFC)*, Mar. 2019, p. W1D.4.
- [179] Y. Li, M. Wu, X. Du, T. Song, and P. Kam, “A refinement to the Viterbi-Viterbi carrier phase estimator and an extension to the case with a Wiener carrier phase process,” *IEEE Access*, vol. 7, pp. 78 170–78 184, Jun. 2019.
- [180] V. Rozentel, D. Kong, B. Corcoran, D. Mello, and A. J. Lowery, “Filtered carrier phase estimator for high-order QAM optical systems,” *IEEE/OSA Journal of Lightwave Technology*, vol. 36, no. 14, pp. 2980–2993, Jul. 2018.
- [181] T. Sasai, A. Matsushita, M. Nakamura, S. Okamoto, F. Hamaoka, and Y. Kisaka, “Laser phase noise tolerance of uniform and probabilistically shaped QAM signals for high spectral efficiency systems,” *IEEE/OSA Journal of Lightwave Technology*, vol. 38, no. 2, pp. 439–446, Jan. 2020.
- [182] T. Yang, C. Shi, X. Chen, M. Zhang, Y. Ji, F. Hua, and Y. Chen, “Linewidth-tolerant and multi-format carrier phase estimation schemes for coherent optical m-QAM flexible transmission systems,” *Optics Express*, vol. 26, no. 8, pp. 10 599–10 615, Apr. 2018.
- [183] J. C. M. Diniz, Q. Fan, S. M. Ranzini, F. N. Khan, F. D. Ros, D. Zibar, and A. P. T. Lau, “Low-complexity carrier phase recovery based on principal component analysis for square-QAM modulation formats,” *Optics Express*, vol. 27, no. 11, pp. 15 617–15 626, May 2019.
- [184] T. T. Nguyen, S. T. Le, M. Wuilpart, and P. Mégret, “Experimental demonstration of a low-complexity phase noise compensation for CO-OFDM systems,” *IEEE Photonics Technology Letters*, vol. 30, no. 16, pp. 1467–1470, Aug. 2018.
- [185] W. Ryan and S. Lin, *Channel Codes: Classical and Modern*. Cambridge University Press, 2009.
- [186] S. M. Kay, *Fundamentals of Statistical Signal Processing: Estimation Theory*. Upper Saddle River, NJ, USA: Prentice-Hall, Inc., 1993.

- 
- [187] A. P. Dempster, N. M. Laird, and D. B. Rubin, "Maximum likelihood from incomplete data via the EM algorithm," *Journal of the Royal Statistical Society. Series B (Methodological)*, vol. 39, no. 1, pp. 1–38, 1977.
- [188] M. J. Beal, "Variational algorithms for approximate Bayesian inference," Ph.D. dissertation, University College London, 2003.
- [189] F. R. Kschischang, B. J. Frey, and H.-A. Loeliger, "Factor graphs and the sum-product algorithm," *IEEE Transactions on Information Theory*, vol. 47, no. 2, pp. 498–519, Feb. 2001.
- [190] A. Doucet, A. Smith, N. de Freitas, and N. Gordon, *Sequential Monte Carlo Methods in Practice*, ser. Information Science and Statistics. Springer New York, 2001.
- [191] S. Särkkä, *Bayesian Filtering and Smoothing*, 1st ed. Cambridge, UK: Cambridge University Press, 2013.
- [192] A. J. Viterbi and A. M. Viterbi, "Nonlinear estimation of PSK-modulated carrier phase with application to burst digital transmission," *IEEE Transactions on Information Theory*, vol. 29, no. 4, pp. 543–551, Jul. 1983.
- [193] P. Zhang, H. Ren, M. Gao, J. Lu, Z. Le, Y. Qin, and W. Hu, "Low-complexity blind carrier phase recovery for C-mQAM coherent systems," *IEEE Photonics Journal*, vol. 11, no. 1, p. 7200214, Feb. 2019.
- [194] M. Xiang, S. Fu, L. Deng, M. Tang, P. Shum, and D. Liu, "Low-complexity feed-forward carrier phase estimation for M-ary QAM based on phase search acceleration by quadratic approximation," *Optics Express*, vol. 23, no. 15, pp. 19 142–19 153, Jul. 2015.
- [195] C. Xie, S. Fu, J. Lu, L. Deng, M. Tang, and D. Liu, "Simplified blind phase search for low-complexity carrier phase estimation of M-ary QAM format," in *Proc. Asia Communications and Photonics Conference (ACPC)*, Nov. 2017, p. Su3B.6.
- [196] T.-H. Nguyen, S.-P. Gorza, J. Louveaux, and F. Horlin, "Low-complexity blind phase search for filter bank multicarrier offset-QAM optical fiber systems," in *Proc. Signal Processing in Photonic Communications (SPPCom)*, Jul. 2016, p. SpW2G.2.
- [197] F. Rice, M. Rice, and B. Cowley, "A new algorithm for 16QAM carrier phase estimation using QPSK partitioning," *Digital Signal Processing*, vol. 12, no. 1, pp. 77–86, Jan. 2002.
- [198] Y. Mori, C. Zhang, K. Igarashi, K. Katoh, and K. Kikuchi, "Phase-noise tolerance of optical 16-QAM signals demodulated with decision-directed carrier-phase estimation," in *Proc. Optical Fiber Communication Conference (OFC)*, Mar. 2009.

- [199] Q. Xiang, Y. Yang, Q. Zhang, and Y. Yao, “Low complexity, modulation-transparent and joint polarization and phase tracking scheme based on the nonlinear principal component analysis,” *Optics Express*, vol. 27, no. 13, pp. 17 968–17 978, Jun. 2019.
- [200] W. J. Weber, “Differential encoding for multiple amplitude and phase shift keying systems,” *IEEE Transactions on Communications*, vol. 26, no. 3, pp. 385–391, Mar. 1978.
- [201] M. A. Castrillón, D. A. Morero, and M. R. Hueda, “Carrier phase recovery without pilot symbols for non-differential coherent receivers,” in *Proc. Optical Fiber Communication Conference (OFC)*, Mar. 2016, p. Tu3K.4.
- [202] H. Cheng, Y. Li, F. Zhang, J. Wu, J. Lu, G. Zhang, J. Xu, and J. Lin, “Pilot-symbols-aided cycle slip mitigation for DP-16QAM optical communication systems,” *Optics Express*, vol. 21, no. 19, pp. 22 166–22 172, Sep. 2013.
- [203] D. S. Millar, R. Maher, D. Lavery, T. Koike-Akino, M. Pajovic, A. Alvarado, M. Paskov, K. Kojima, K. Parsons, B. C. Thomsen, S. J. Savory, and P. Bayvel, “Design of a 1 Tb/s superchannel coherent receiver,” *IEEE/OSA Journal of Lightwave Technology*, vol. 34, no. 6, pp. 1453–1463, Mar. 2016.
- [204] R. Maher, K. Croussore, M. Lauer mann, R. Going, X. Xu, and J. Rahn, “Constellation shaped 66 GBd DP-1024QAM transceiver with 400 km transmission over standard SMF,” in *Proc. European Conference on Optical Communication (ECOC)*, Sep. 2017, p. Th.PDP.B.2.
- [205] V. Kamalov, L. Jovanovski, V. Vusirikala, S. Zhang, F. Yaman, K. Nakamura, T. Inoue, E. Mateo, and Y. Inada, “Evolution from 8QAM live traffic to PS 64-QAM with neural-network based nonlinearity compensation on 11000 km open sub-sea cable,” in *Proc. Optical Fiber Communication Conference (OFC)*, Mar. 2018, p. Th4D.5.
- [206] J.-X. Cai, H. G. Batshon, M. V. Mazurczyk, O. V. Sinkin, D. Wang, M. Paskov, C. R. Davidson, W. W. Patterson, A. Turukhin, M. A. Bolshtyansky, and D. G. Foursa, “51.5 Tb/s capacity over 17,107 km in C+L bandwidth using single-mode fibers and nonlinearity compensation,” *IEEE/OSA Journal of Lightwave Technology*, vol. 36, no. 11, pp. 2135–2141, Jun. 2018.
- [207] T. T. Nguyen, S. T. Le, R. Nissel, M. Wuilpart, L. Van Compernelle, and P. Mégret, “Pseudo-pilot coding based phase noise estimation for coherent optical FBMC-OQAM transmissions,” *IEEE/OSA Journal of Lightwave Technology*, vol. 36, no. 14, pp. 2859–2867, Jul. 2018.

- 
- [208] M. Mazur, J. Schröder, A. Lorences-Riesgo, T. Yoshida, M. Karlsson, and P. A. Andrekson, "Overhead-optimization of pilot-based digital signal processing for flexible high spectral efficiency transmission," *Optics Express*, vol. 27, no. 17, pp. 24 654–24 669, Aug. 2019.
- [209] A. F. Alfredsson, R. Krishnan, and E. Agrell, "Joint-polarization phase-noise estimation and symbol detection for optical coherent receivers," *IEEE/OSA Journal of Lightwave Technology*, vol. 34, no. 18, pp. 4394–4405, Sep. 2016.
- [210] R. E. Kalman, "A new approach to linear filtering and prediction problems," *ASME Journal of Basic Engineering*, vol. 82, no. 1, pp. 35–45, Mar. 1960.
- [211] M. Pajovic, D. S. Millar, T. Koike-Akino, R. Maher, D. Lavery, A. Alvarado, M. Paskov, K. Kojima, K. Parsons, B. C. Thomsen, S. J. Savory, and P. Bayvel, "Experimental demonstration of multi-pilot aided carrier phase estimation for DP-64QAM and DP-256QAM," in *Proc. European Conference on Optical Communication (ECOC)*, Sep. 2015, p. Mo.4.3.3.
- [212] R. Krishnan, M. R. Khanzadi, T. Eriksson, and T. Svensson, "Soft metrics and their performance analysis for optimal data detection in the presence of strong oscillator phase noise," *IEEE Transactions on Communications*, vol. 61, no. 6, pp. 2385–2395, Jun. 2013.
- [213] A. C. Bordonalli, M. J. Fice, and A. J. Seeds, "Optical injection locking to optical frequency combs for superchannel coherent detection," *Optics Express*, vol. 23, no. 2, pp. 1547–1557, Jan. 2015.
- [214] D. V. Souto, B.-E. Olsson, C. Larsson, and D. A. A. Mello, "Joint-polarization and joint-subchannel carrier phase estimation for 16-QAM optical systems," *IEEE/OSA Journal of Lightwave Technology*, vol. 30, no. 20, pp. 3185–3191, Oct. 2012.
- [215] R. S. Luís, B. J. Puttnam, J.-M. Delgado Mendinueta, W. Klaus, Y. Awaji, and N. Wada, "Comparing inter-core skew fluctuations in multi-core and single-core fibers," in *Proc. Conference on Lasers and Electro-Optics (CLEO)*, May 2015, p. SM2L.5.
- [216] R. Krishnan, G. Colavolpe, A. Graell i Amat, and T. Eriksson, "Algorithms for joint phase estimation and decoding for MIMO systems in the presence of phase noise and quasi-static fading channels," *IEEE Transactions on Signal Processing*, vol. 63, no. 13, pp. 3360–3375, Jul. 2015.
- [217] A. O. Isikman, H. Mehrpouyan, A. A. Nasir, A. Graell i Amat, and R. A. Kennedy, "Joint phase noise estimation and data detection in coded multi-input–multi-output systems," *IET Communications*, vol. 8, no. 7, pp. 981–989, May 2014.

- [218] H. Mehrpouyan, A. A. Nasir, S. D. Blostein, T. Eriksson, G. K. Karagiannidis, and T. Svensson, “Joint estimation of channel and oscillator phase noise in MIMO systems,” *IEEE Transactions on Signal Processing*, vol. 60, no. 9, pp. 4790–4807, Sep. 2012.
- [219] M. Simko, P. S. R. Diniz, Q. Wang, and M. Rupp, “Adaptive pilot-symbol patterns for MIMO OFDM systems,” *IEEE Transactions on Wireless Communications*, vol. 12, no. 9, pp. 4705–4715, Sep. 2013.
- [220] M. D. Larsen, G. Seco-Granados, and A. L. Swindlehurst, “Pilot optimization for time-delay and channel estimation in OFDM systems,” in *Proc. International Conference on Acoustics, Speech, and Signal Processing (ICASSP)*, May 2011, pp. 3564–3567.
- [221] Y. Zhang, J. Liu, S. Feng, and P. Zhang, “Pilot design for phase noise mitigation in millimeter wave MIMO-OFDM systems,” in *Proc. Vehicular Technology Conference (VTC)*, Jun. 2017.
- [222] X. Ma, H. Zhang, X. Yao, and D. Peng, “Pilot-based phase noise, IQ mismatch, and channel distortion estimation for PDM CO-OFDM system,” *IEEE Photonics Technology Letters*, vol. 29, no. 22, pp. 1947–1950, Nov. 2017.
- [223] J. Bhatti and M. Moeneclaey, “Influence of pilot symbol configuration on data-aided phase noise estimation from a DCT basis expansion,” in *Proc. International Networking and Communications Conference*, May 2008, pp. 79–84.